Nonlinear Polymer Nanocomposite for Field Grading in Medium-Voltage Power Converters under High-Altitude and Humid Environments

Zachary Zintak

Thesis submitted to the Faculty of the

Virginia Polytechnic Institute and State University

in partial fulfillment of the requirements for the degree of

Master of Science

in

Materials Science and Engineering

Guo-Quan Lu, Chair

Khai D. T. Ngo

Chenggang Tao

December 2, 2025

Blacksburg, Virginia

Keywords: Power module insulation, Partial discharge, Humidity, E-field reduction, Nonlinear resistive polymer nanocomposite, High altitude.

Copyright 2025, Zachary Zintak

Nonlinear Polymer Nanocomposite for Field Grading in Medium-Voltage Power Converters under High-Altitude and Humid Environments

Zachary Zintak

(ABSTRACT)

This thesis presents the development and characterization of a nonlinear resistive polymer nanocomposite (PNC) coating designed to enhance insulation within medium-voltage (MV) power modules and suppress flashover on printed-circuit boards (PCBs) at high altitudes. Electric field simulations of the triple-point (TP) region revealed strong E-field intensification at conductor-ceramic-silicone and conductor-FR4-air interfaces, leading to premature partial discharges and breakdown. To mitigate these effects, a PNC coating composed of a polymer matrix with dispersed conductive nanoparticles was applied as a conformal field-grading layer. Electrostatic force microscopy (EFM) measurements exhibit an average distance of 135 nm between nanoparticles within the polymer matrix. Finite element simulations conducted in COMSOL demonstrated that the nonlinear conductivity of the PNC effectively redistributed the local electric field, reducing the peak intensity at the TP by approximately 50% compared to an uncoated interface. Experimental validation through partial discharge inception voltage (PDIV) and breakdown voltage (BV) tests confirmed that the PNC coating increased surface flashover voltage by approximately 30% under both ambient and low-pressure conditions when exposed to air. Humidity aging and condensation tests were performed to assess the long-term reliability of the coating within power modules. The PNC maintained its insulation improvement ability under prolonged high-humidity exposure, showing no measurable degradation in insulation strength. Overall,

this work demonstrates a robust and environmentally stable nonlinear coating for surface field grading in MV power modules and converters. The PNC provides a promising pathway toward improving partial discharge immunity and insulation reliability in high-power, high-voltage electronic packaging applications.

Nonlinear Polymer Nanocomposite for Field Grading in Medium-Voltage Power Converters under High-Altitude and Humid Environments

Zachary Zintak

(GENERAL AUDIENCE ABSTRACT)

This thesis presents the development of a polymer nanocomposite coating that improves electrical insulation and prevents breakdown in medium-voltage power systems. These systems are increasingly used in electric vehicles, aircraft, and renewable energy converters, where compact, reliable insulation is essential, especially at high altitudes where electrical breakdown is more likely to occur. In these environments, strong electric fields can form at specific regions called triple points, where different materials meet, leading to surface discharges and insulation failure. To address this challenge, a specially formulated coating made of a polymer mixed with conductive nanoparticles was developed and applied as a thin, conformal layer over these triple points. This coating has a unique property called nonlinear resistivity, meaning its ability to conduct electricity changes with the strength of the electric field, allowing it to smooth out localized field concentrations and prevent discharges. Simulations and experiments confirmed that the coating reduced electric field stress by about 50% and increased surface flashover voltage by roughly 30% under both normal and low-pressure conditions. The coating's reliability was also tested under high-humidity and condensation conditions to simulate real-world operating environments within power modules. Results showed that the material maintained its insulating performance and did not degrade after prolonged exposure. Overall, this work demonstrates a durable and adaptive

insulation coating that can significantly enhance the safety and reliability of next-generation medium-voltage power modules and high-altitude electronic systems.

Acknowledgments

I would like to express my gratitude to everyone that helped me throughout my journey of completing this thesis. I would like to first like to thank my advisor Dr. Guo-Quan Lu. His guidance over the years has been invaluable and has helped me grow significantly as a researcher and engineer. What I have learned under his tutelage will continue to assist me throughout my life and career. Next, I would like to thank my committee members Dr. Khai Ngo and Dr. Chenggang Tao. It was a great pleasure to be a part of the High-Density Integration (HDI) Mini-consortium under Dr. Ngo during my time at Virginia Tech and learn characterization techniques under Dr. Tao. I give special thanks to Dr. Kaixuan Li, who had been a fantastic mentor to me during my first year in the graduate school and assisted me to build momentum. I would also like to thank Mr. Peiyuan Sun and Mr. Sidh Jaddu for their contribution to this work in the characterization and FEA simulations respectively. Further thanks goes to the Virginia Tech and Center for Power Electronics Systems (CPES) staff that supported me throughout my journey: Ms. Cindy Purdue, Ms. Amy Hill, Dr. Thomas Staley, Dr. Carlos Scuchicital, Mr. David Gilham, Mr. Dennis Grove, Mr. Neil Croy, Ms. Yan Sun, Ms. Nina Jaworski, and Ms. Brandy Grim. It has been a great experience working with and learned from my colleagues and friends: Mr. Joshua Gardner, Mr. Andrew Zhang, Mr. Yancheng Chen, Mr. Juan Vascones, Mr. Mihn Ngo, Mr. Aakash Kamalapur, Mr. David Nam, Mr. Matthias Spieler, Mr. Tyler McGrew, Ms. Yan Liang, Mr. Promit Datta, Mr. Matthew Porter, Mr. Steven Ash, Ms. Margarett Paczkowski, Mr. Abhinav Soni, and many more. I want to acknowledge the CPES HDI Mini-consortium, Advanced Research Projects Agency-Energy (ARPA-E) of the U.S. Department of Energy under DE-AR0001914, the Office of Naval Research (ONR) NEPTUNE under award number N000142512238, and

LaunchBay LLC for financially supporting my research during my master's study. Lastly, I would like to thank my parents, Mr. George Zintak and Ms. Madalynn Zintak for their unconditional support and my fiancee Ms. Heather Korzun for her companionship.

Contents

List of Figures xi

List of Tables xiv

1 Introduction 1

1.1 Background and Motivation 1

1.1.1 Electrification and Medium-Voltage Power Electronics 1

1.1.2 Partial Discharge and Breakdown at Triple Points 2

1.1.3 High-Altitude Insulation Challenges 4

1.1.4 Humid Environment Insulation Degradation 5

1.1.5 Field Grading and Nonlinear Resistive Materials 6

1.2 Significance of This Work 6

1.3 Thesis Structure 7

2 Characterization of the Polymer Nanocomposite Coating 9

2.1 Experimental Setup 9

2.1.1 Sample Preparation 9

2.1.2 SEM and Surface Imaging 10

2.1.3 EFM Overview 11

2.2 Results and Discussion 12
2.2.1 Cross-Section SEM and Surface Morphology 12
2.2.2 EFM Particle Distribution 13
2.3 Conclusion 14

3 Effect of Conformal Coating on Electric Field Around PCB Electrode in Air: Simulation 17

3.1 Simulation Setup 17
3.1.1 Geometry 17
3.1.2 Materials 18
3.2 Results and Discussion 19
3.3 Conclusion 21

4 PNC Enhanced Flashover Voltage of PCBs at High Elevation 23

4.1 Experimental Setup 24
4.1.1 Sample Preparation 24
4.1.2 PDIV and Flashover Voltage Measurement Setup 25
4.1.3 Low-Pressure Flashover Voltage Measurement 25
4.2 Results and Discussion 26
4.2.1 Ambient Air PDIV and BV Results 26
4.2.2 Breakdown Voltage Testing in Reduced Pressures 28

4.3 Conclusion 29

5 Effect of Moisture on PNC Field-Grading in MV Power Modules 35

5.1 Experimental Setup 36

5.1.1 Mass Change Measurements of DBC Substrates 36

5.1.2 PDIV Measurements of DBC Substrates 37

5.1.3 Salt Fog Corrosion of Coated DBC Substrates 38

5.2 Results and Discussion 39

5.2.1 Mass Change Results 39

5.2.2 PDIV Results 40

5.2.3 Salt Fog Corrosion PDIV Results 40

5.3 Conclusion 41

6 Summary 44

6.1 Material Characterization and Morphology 44

6.2 Electric Field Simulation of Triple Points 45

6.3 Surface Flashover and Low-Pressure Performance 46

6.4 Humidity Aging in Encapsulated Modules 46

6.5 Overall Findings and Future Outlook 47

List of Figures

1.1 Comparison of power device on-resistance and breakdown voltage [2]. 2

1.2 (a) A sharp protrusion left by chemical etching of a direct-bonded copper (DBC) substrate [27]. (b) An electrical tree formed within a power module's encapsulation material after experiencing PD. 3

1.3 Paschen's curve experimental data for air [21]. 4

2.1 Uncured PNC solution. 10

2.2 (a) PCB sample with PNC applied to the smaller upper electrode. (b) PNC applied to the surface of diced silicon wafers. 11

2.3 NAP mode conducted by the AFM. Topography is first measured (1), then the probe follows the topography a set height Δz above the measured topography (2). 12

2.4 Cross-section SEM image of PCB sample. Lower region shows the FR4 and the mound to the right shows the 1 oz copper trace. The darker region surrounding the copper trace shows the PNC with particles distributed throughout. 13

2.5 (a) Height surface image of the PNC coated on a PCB substrate in a 2 mm x 2 mm area. (b) Profile of the surface through the middle of the image shown in (a). 15

2.6 (a) Topography of PNC. (b) NAP phase of PNC, dark dots show nanoparticle locations under 5 V bias. 16

3.1 Geometry of the E-field simulation with a 9.5 mm gap between the HV and GND traces. 18

3.2 FEA simulation results with TP surrounded by air. 20

3.3 FEA simulation results with TP surrounded by the commercial MG material. 20

3.4 FEA simulation results with TP surrounded by air. 21

3.5 FEA simulation results with TP surrounded by air collected in a line 10 μm above the FR4. 22

4.1 PCB sample schematic with a 9.5 mm gap between the HV and GND electrodes. 24

4.2 PDIV measurement setup with PD free HV source, coupling capacitor, MPD-600 detection system and sample under test. Circuit schematic is shown on the top left. 26

4.3 Acrylic vacuum chamber used to emulate high-altitude environments. 27

4.4 (a) PDIV results in ambient pressure. (b) Corona at the TP of the HV electrode. 31

4.5 (a) BV results in ambient pressure. (b) Arc connecting the HV and GND electrodes. 32

4.6 BV results in 50 kPa conditions within the vacuum chamber. Samples exhibit arc as seen in Fig. 4.5b. 33

4.7 BV results in 20 kPa conditions within the vacuum chamber. 34

5.1 (a) Schematic of alumina DBC test coupon. (b) Photo of a coated DBC substrate with silicone encapsulation 37

5.2 PDIV measurement setup with PD free HV source, coupling capacitor, MPD-600 detection system and sample under test. 38

5.3 Average percent mass change for encapsulated DBC samples for 200/500 hr aging times. 39

5.4 Average PDIV for both gel (a) and elastomer (b) encapsulated gel DBC samples for 200/500 hr aging times. 42

5.5 Percent improvement of PDIV from uncoated to coated DBC substrates for each encapsulation material and aging time. 43

5.6 Average PDIV for elastomer encapsulated gel DBC samples before and after salt fog aging. 43

List of Tables

3.1 Materials properties used in E-field simulation. 18

3.2 Values used in Equation 3.1. 19

List of Abbreviations

AC Alternating Current

AFM Atomic Force Microscopy

BV Breakdown Voltage

DBC Direct-Bonded Copper

DC Direct Current

DUT Device Under Test

E-field Electric Field

EFM Electrostatic Force Microscopy

EV Electric Vehicle

GaN Gallium Nitride

H^3TRB High Humidity, High Temperature Reverse Bias

HV High-Voltage

MV Medium-Voltage

NAP Non-contact AC Potential

PCB Printed-Circuit Board

PD Partial Discharge

PDIV Partial Discharge Inception Voltage

PNC Polymer Nanocomposite

RH Relative Humidity

SEM Scanning Electron Microscopy

SiC Silicon Carbide

THB Temperature, Humidity, Bias

TP Triple Point

WBG Wide-Bandgap

Chapter 1

Introduction

1.1 Background and Motivation

1.1.1 Electrification and Medium-Voltage Power Electronics

Rapid electrification of transportation, renewable energy systems, and industrial power conversion has driven the need for reliable medium-voltage (MV) power modules capable of handling higher voltages, temperatures, and switching frequencies [1]. Electric vehicles (EVs), electric aircraft and grid-tied converters increasingly rely on compact and reliable power electronics to enable clean and sustainable energy technologies.

Wide-bandgap (WBG) semiconductors such as silicon carbide (SiC) and gallium nitride (GaN) have allowed us to achieve these advances due to their superior electrical and thermal performance compared to traditional silicon devices [2]. They allow for higher blocking voltages, seen in Fig. 1.1, and faster switching speeds, which reduce conduction and switching losses and enable higher power density designs [3–9]. As MV SiC power devices rated above 2 kV become more common in electric traction and aerospace systems, the demand for compact insulation solutions with high reliability has become increasingly critical [10–15].

While WBG-based power modules enable improved system efficiency, they also impose new challenges in insulation design. Higher operating voltages produce intensified electric

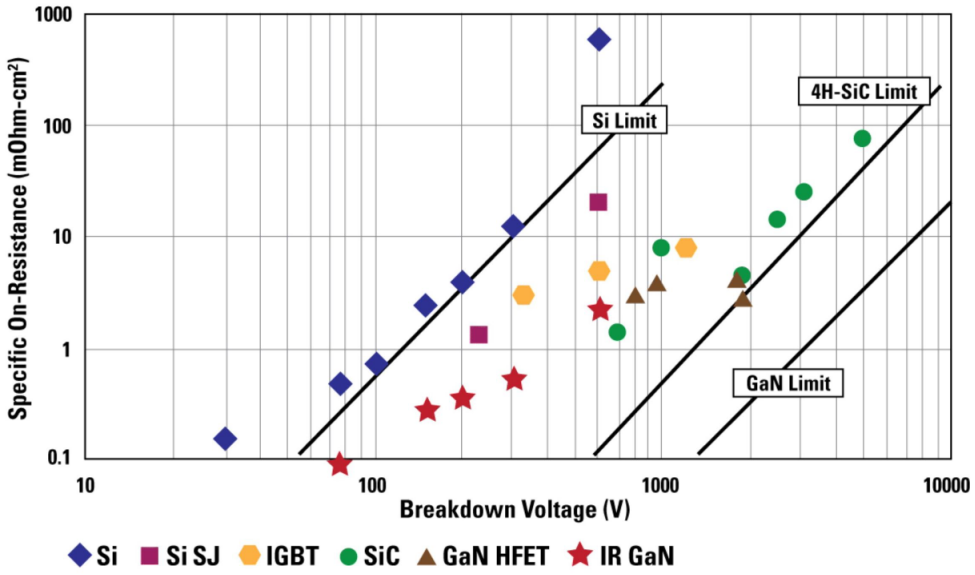

Figure 1.1: Comparison of power device on-resistance and breakdown voltage [2].

fields within encapsulants, substrates, and at air-solid interfaces, often leading to partial discharge or dielectric breakdown [16–20]. These failure modes are particularly problematic in high-altitude and high-humidity environments, where reduced air pressure lowers the breakdown voltage of air and moisture can invade insulation materials, increasing the risk of partial discharge and insulation degradation [21, 22].

1.1.2 Partial Discharge and Breakdown at Triple Points

Partial discharge refers to a localized electrical discharge that only partially bridges conductors within a dielectric. As partial discharge events occur, the dielectric begins to degrade and can eventually lead to full dielectric breakdown [19, 23–25]. Breakdown refers to the process that occurs when a dielectric is subjected to a high enough voltage that it suddenly becomes a conductor and current can freely pass through it. Both processes often begin with localized electric field intensification at geometric discontinuities and material boundaries known as triple points (TPs) where a conductor and two insulators meet. At

these locations, not only are these rapid material property changes, but TPs are also regions more prone to defects, such as sharp corners or voids within the dielectric as shown in Fig. 1.2a [19, 20, 26, 27].

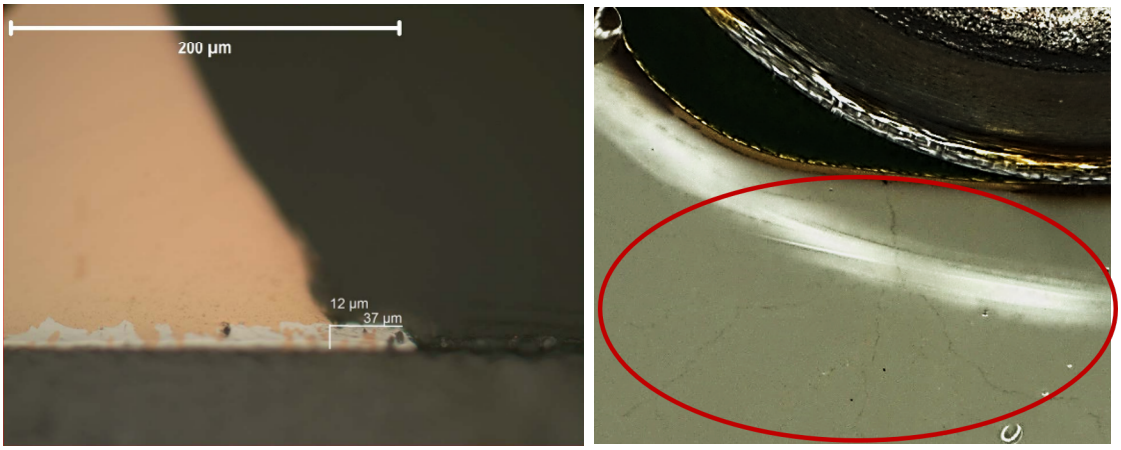

(a) (b)

Figure 1.2: (a) A sharp protrusion left by chemical etching of a direct-bonded copper (DBC) substrate [27]. (b) An electrical tree formed within a power module's encapsulation material after experiencing PD.

In power modules and printed-circuit boards (PCBs), TPs are commonly found at the terminations of the conductors. At these locations, nonuniform field distributions can exceed 3 times the average electric field (E-field) within the dielectric, leading to partial discharge [18]. Once initiated, discharges can erode the insulation or inject charges into the dielectric, seen in Fig. 1.2b, eventually resulting in catastrophic breakdown [25].

Some mitigation strategies involve geometric field control (such as rounded electrodes) [27], trench structures [28], thicker dielectrics [29], or field-plates [30]. However, these solutions increase package volume, increase manufacturing cost and complexity, or are not linearly effective. Therefore, a material-based approach that can dynamically respond to the electric field distribution is desirable for future MV insulation systems.

1.1.3 High-Altitude Insulation Challenges

Power electronic converters designed for aerospace, such as electric aircraft and satellites, must operate under reduced atmospheric pressure [10, 21]. As altitude increases, the density of air molecules decreases, lowering the dielectric strength of air and consequently the voltage at which electrical breakdown occurs [31]. This relationship is described by Paschen's Law, depicted in Fig. 1.3, which shows that the breakdown voltage of air decreases with decreasing pressure-distance [32, 33]. At pressures typical of altitudes between 5 and 15 km, the breakdown voltage can be less than half that at sea level.

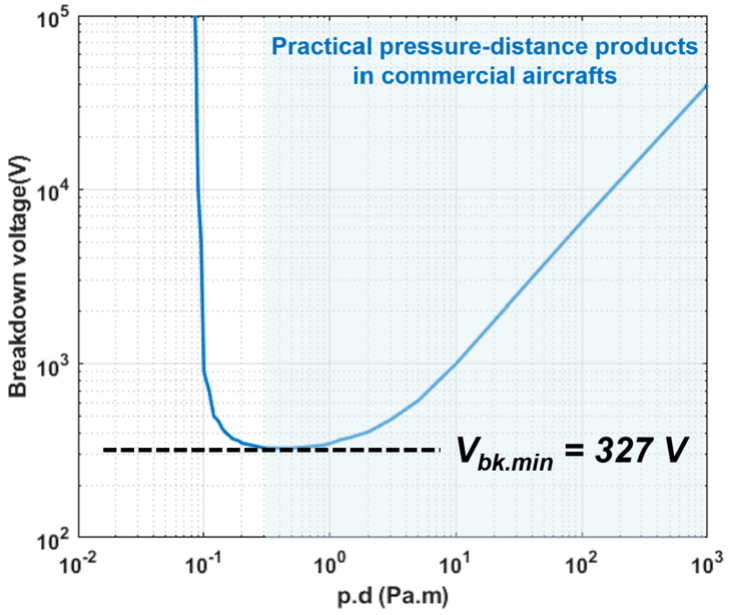

Figure 1.3: Paschen's curve experimental data for air [21].

Under these conditions, surface flashover, a form of breakdown that travels along the interface between a solid insulator and air, becomes a dominant failure mechanism [34]. The reduced dielectric strength allows small irregularities or charge accumulation at TPs to trigger premature discharge. Once initiated, surface discharges can extend across the surface and evolve into a complete flashover, permanently degrading the insulation material.

High-altitude environments therefore pose significant challenges to maintaining insulation reliability in MV converters and printed-circuit boards. To mitigate these effects, an increase in the creepage distances between conductors is a typical method to mitigate this problem. However, this method increases the volume and weight of the system.

1.1.4 Humid Environment Insulation Degradation

Power electronic converters are often being deployed in harsh and humid environments, such as offshore wind turbines, railway traction systems, and electric vehicles. In these systems, long-term exposure to moisture and condensation can impact the electrical insulation materials used for encapsulation [22, 35, 36]. As the industry moves toward higher voltage operation and denser packaging, environmental reliability has become one of the most critical challenges to ensuring safe and stable performance over the converter's lifetime.

Silicone gels are widely used as encapsulants in MV power modules due to their excellent flexibility, thermal stability, and dielectric strength. Their soft, conformable nature allows them to fill voids and protect interconnects and chips from vibration and mechanical stress. However, silicone materials are permeable to moisture, and studies have shown that they can absorb water molecules from the surrounding atmosphere during extended operation in humid conditions [37].

Once absorbed, moisture can alter the electrical and chemical properties of the encapsulant. Reports in [22, 35, 36] indicate that prolonged humidity exposure leads to a reduction in electrical resistivity and increased leakage current. The formation of conductive pathways along the polymer–filler interfaces. Additionally, under high-field stress, the absorbed water can promote partial discharges at voids or interfaces, accelerating electrical aging.

1.1.5 Field Grading and Nonlinear Resistive Materials

Nonlinear resistive materials exhibit field-dependent conductivity, allowing them to act as self-regulating field-grading layers. When the local electric field increases, their conductivity rises, redistributing charge and reducing the field gradient in high-stress regions [38–40]. This concept has been widely used employing ZnO-based ceramics as filler materials [41, 42]. However, these rigid and brittle materials are unsuitable for conformal coatings in power modules or PCB applications.

The polymer nanocomposite (PNC) offers a flexible alternative by combining an insulating polymer matrix with dispersed conductive nanoparticles. The resulting material maintains a low viscosity $< 10{,}000$ cps, allowing for it to be applied to tight regions such as TPs [16]. Recent studies on the PNC has shown that nanoparticle inclusion can enhance partial discharge resistance, increasing partial discharge inception voltage by $> 85\%$ when applied to the TPs of direct-bonded copper substrates [43–45]. Despite these advantages, limited work has focused on exposing the PNC coating to reduced pressure or humid environments.

1.2 Significance of This Work

This research introduces and investigates the application of the PNC coating as a insulation enhancement layer for MV power modules and PCBs within reduced pressure and humid environments.

Finite element simulations were performed to analyze the electric field distribution at TP regions with and without the coating. The results demonstrated that the nonlinear conductivity of the PNC can effectively redistribute the field, reducing peak electric field

stress by approximately 50% compared to uncoated surfaces. Experimental flashover testing confirmed that the PNC improved surface insulation performance by roughly 30% in both normal and low-pressure environments.

In addition to electrical performance, this work investigates the environmental durability of the PNC through humidity aging testing. The PNC maintained its insulating performance after prolonged exposure to high humidity, demonstrating potential for use in real-world MV applications where moisture is unavoidable such as off-shore wind farms.

By integrating materials characterization, electrical testing, and finite element simulation, this thesis provides a comprehensive understanding of how nonlinear nanocomposite coatings can be used to enhance field control and insulation reliability in next-generation MV power electronics.

1.3 Thesis Structure

This thesis is organized into six chapters.

Chapter 1 introduces the motivation for this project. Driven by WBG semiconductors, the need for improved insulation in MV systems is described and the problem of partial discharge and breakdown is emphasized. Nonlinear resistive materials for field grading and reliability enhancement are highlighted as a promising material for addressing this need.

Chapter 2 presents the electrical characterization of the PNC coating, including surface morphology and nanoparticle distribution analysis using electrostatic force microscopy (EFM) data.

Chapter 3 details electric field modeling of triple points using finite element simulation, comparing coated and uncoated configurations to evaluate field suppression mechanisms in

air and within a power module.

Chapter 4 describes partial discharge inception voltage (PDIV) and breakdown voltage (BV) testing under both ambient and reduced-pressure conditions. Sample configuration and testing for air environments is detailed in this chapter.

Chapter 5 investigates humidity aging reliability of the PNC within a power module. Aging procedure and sample test flow are described within this chapter.

Chapter 6 summarizes the key findings, highlights the contributions of this research, and discusses future work toward integrating PNC coatings into commercial MV module packaging and power converter systems.

Chapter 2

Characterization of the Polymer Nanocomposite Coating

Understanding the electrical and morphological properties of the PNC coating is essential to ensure the quality of the coating and suppress discharge in medium-voltage insulation systems. The PNC's ability to mitigate electric field intensification depends strongly on its nanoparticle dispersion, microstructure, and cross-sectional analysis.

This chapter presents material characterization study of the PNC coating, focusing on its surface morphology and nanoparticle distribution. Scanning electron microscopy (SEM) and EFM are used to analyze particle dispersion and interfacial structure, while the nonlinear conduction behavior is evaluated through DC current-voltage measurements. Surface topography and roughness are also quantified using profilometry and atomic force microscopy (AFM) to assess coating uniformity and quality.

2.1 Experimental Setup

2.1.1 Sample Preparation

The PNC coating was formulated by dispersing conductive nanoparticles into a polymer matrix to form a low viscosity ($<$ 10,000 cps) paint solution, seen in Fig. 2.1. After creating

the mixture, the solution is degassed to remove trapped air before application. The solution is able to be easily applied via paint brush along TPs.

Figure 2.1: Uncured PNC solution.

For this chapter, there are two different types of samples investigated. For SEM imaging and surface profilometry, PCB samples used for air electrical testing used in 4 are investigated. The TP is investigated on the surface as well as a cross-section. For EFM, the PNC is applied on the surface of a diced silicon wafer, metalized with titanium and silver to make the surface electrically conductive. Each sample was thermally cured at 180°C for forty minutes to promote crosslinking. Both types of samples are seen in fig 2.2.

2.1.2 SEM and Surface Imaging

Scanning electron microscopy (SEM) was used to examine the adhesion, voiding, and thickness at the interface of the PNC coating and the FR4 substrate. SEM imaging was performed on a JEOL JCM-7000 microscope operating at an accelerating voltage of 15 kV and a working distance of approximately 12 mm.

Surface morphology measurements were carried out using a Keyence VK-X3000 3D surface profilometer and Oxford Jupiter XR AFM. The profilometer provided coating thickness

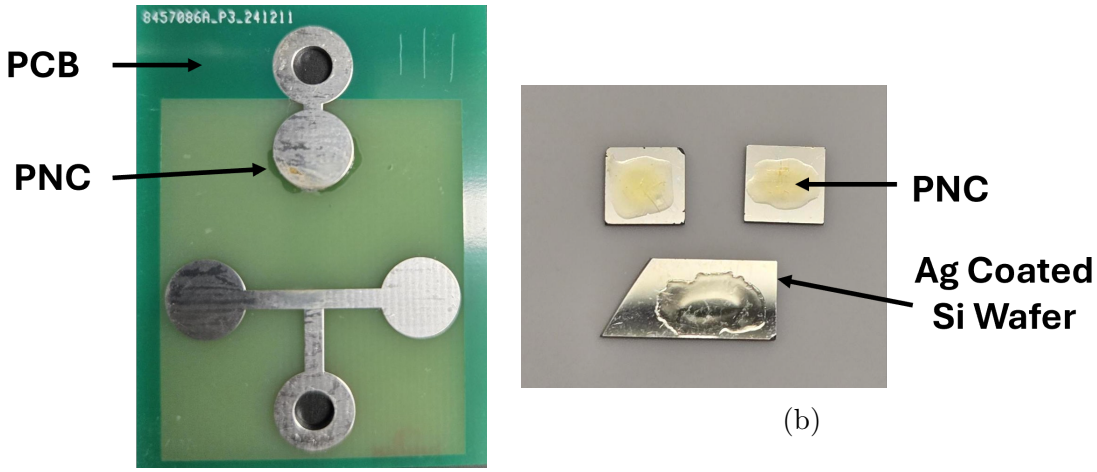

(a) (b)

Figure 2.2: (a) PCB sample with PNC applied to the smaller upper electrode. (b) PNC applied to the surface of diced silicon wafers.

and overall surface profile over a 2 mm scan area, while AFM offered nanoscale surface topography over a 10 μm x 10 μm area in tapping mode.

The average surface roughness (R_a) and root mean square roughness (R_q) were extracted from AFM scans to quantify the coating smoothness. A low R_a value ensures uniform electric field distribution across coated electrodes.

2.1.3 EFM Overview

Electrostatic force microscopy (EFM) was utilized to analyze the nanoscale electrical uniformity and local potential distribution of the PNC coating. Measurements were conducted using the Oxford Jupiter XR AFM in Non-contact AC Potential (NAP) mode.

During EFM scanning, the conductive tip first traces the surface topography in AC mode in air and then re-scans the same line at a constant lift height Δz, following along the previously measured topography, while a DC bias is applied between the tip and the sample. By lifting at this constant height Δz, the cantilever is able to be decoupled from

the topography of the sample and only be affected by electric fields. Phase data shows the electrostatic induced shift in resonance frequency. This technique allows visualization of conductive nanoparticle distribution within the polymer matrix. A visual of the NAP mode utilized by the EFM is pictured in Fig. 2.3.

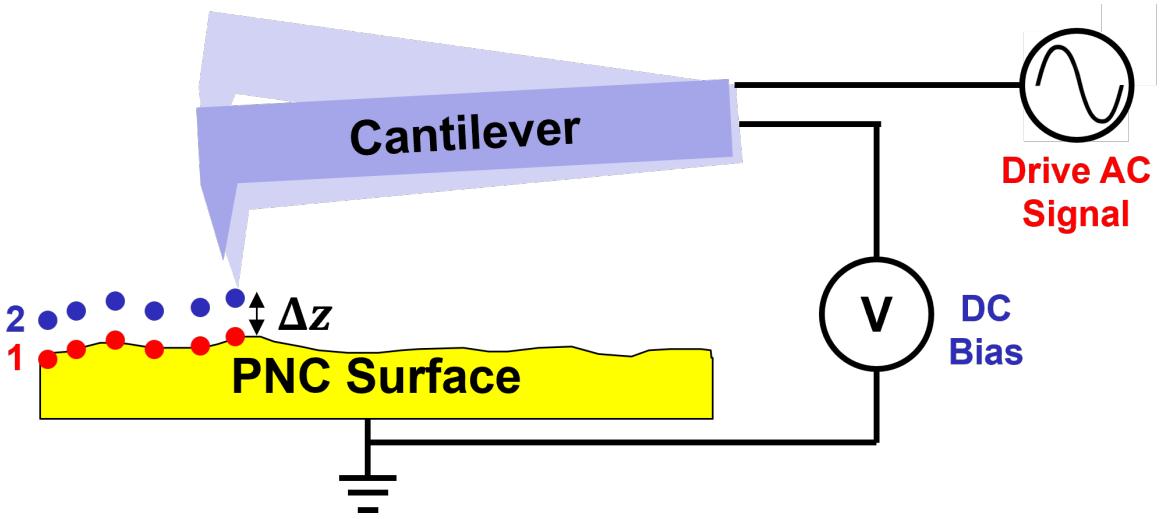

Figure 2.3: NAP mode conducted by the AFM. Topography is first measured (1), then the probe follows the topography a set height Δz above the measured topography (2).

2.2 Results and Discussion

2.2.1 Cross-Section SEM and Surface Morphology

Representative cross-sectional SEM micrographs of the PNC coating are shown in Fig. 2.4. The coating exhibits a dense, continuous structure with no voids or delamination at the interface between the PNC and substrate. The embedded nanoparticles appear well distributed throughout the polymer matrix. From this image, we also measure the thickness of the PNC to be 60 μm at the thickest region to just to the left of the copper trace and 40 μm above the trace.

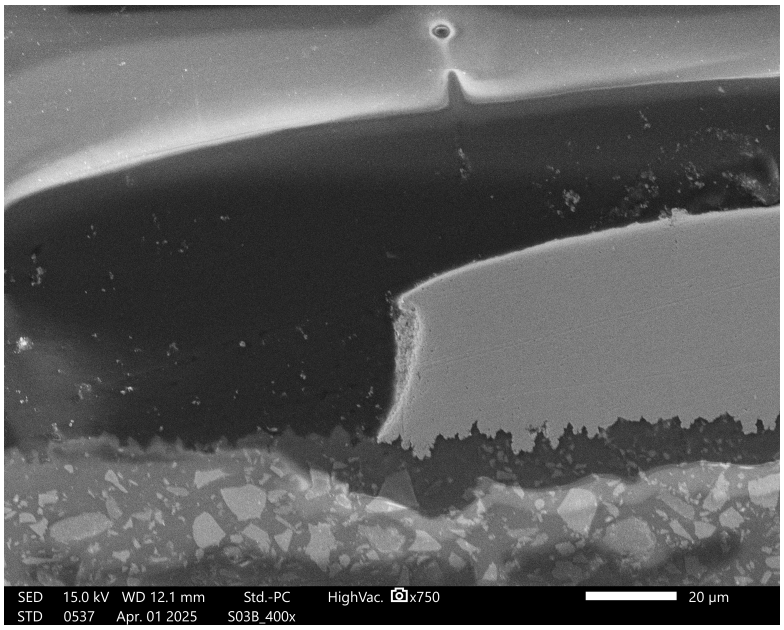

Figure 2.4: Cross-section SEM image of PCB sample. Lower region shows the FR4 and the mound to the right shows the 1 oz copper trace. The darker region surrounding the copper trace shows the PNC with particles distributed throughout.

Fig. 2.5 presents the surface topography of the cured PNC coating on a PCB substrate. Profilometry confirmed an average coating thickness of 60 μm, while AFM measurements yielded an average roughness (R_a) of ~700 pm and an R_q of 1.3 nm in an area of 100 μm^2. AFM topography measurements are included in Fig. 2.6a. The resulting surface remains sufficiently smooth for conformal coverage on copper electrodes and is unlikely to induce additional electric field distortion. These results confirm that the coating process yields a morphologically stable and electrically uniform layer suitable for power module encapsulation and field-grading applications.

2.2.2 EFM Particle Distribution

The EFM measurements provided nanoscale insight into the spatial distribution of nanoparticles within the PNC coating. Fig. 2.6 shows both the topography and the corre-

sponding EFM phase image under an applied 5 V DC bias between the cantilever and PNC surface. The EFM contrast reveals relative dark regions corresponding to local variations in electrostatic potential, which are associated with the conductive nanoparticles dispersed in the polymer. Analysis shows an average distance between from nearest particles of 135 nm, indicative of a homogeneous particle dispersion, consistent with SEM observations. No evidence of large-scale clustering or percolation paths was observed.

2.3 Conclusion

Cross-sectional SEM imaging confirmed uniform nanoparticle dispersion without voids or delamination, while surface morphology measurements showed that the coating maintained a smooth topography ($R_a \approx 700$ pm) suitable for conformal application. EFM analysis revealed nanoscale uniformity in particle distribution.

Overall, the results confirm that the PNC coating combines excellent structural uniformity, validating its potential as a field-grading and surface insulation enhancement material for medium-voltage power modules and high-altitude systems.

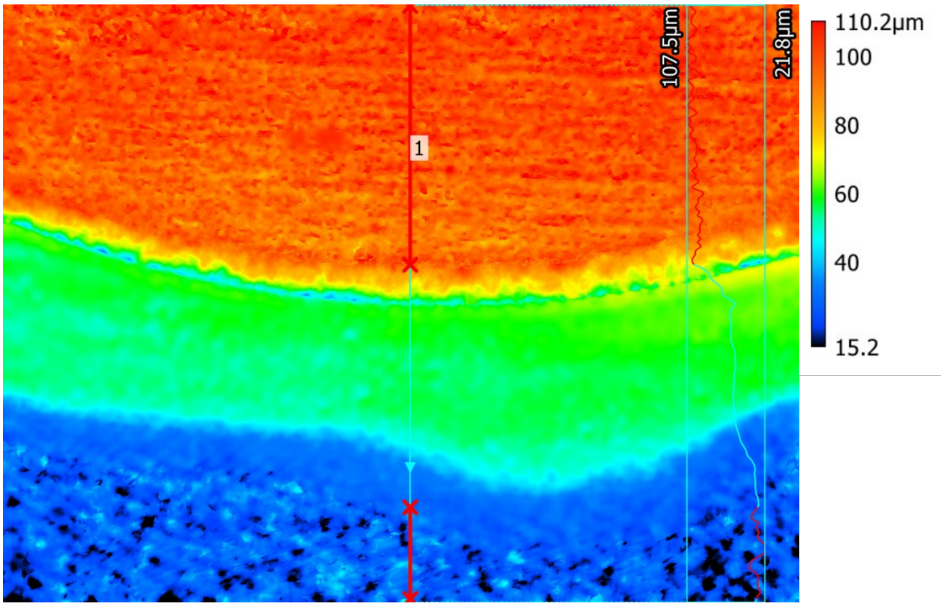

(a)

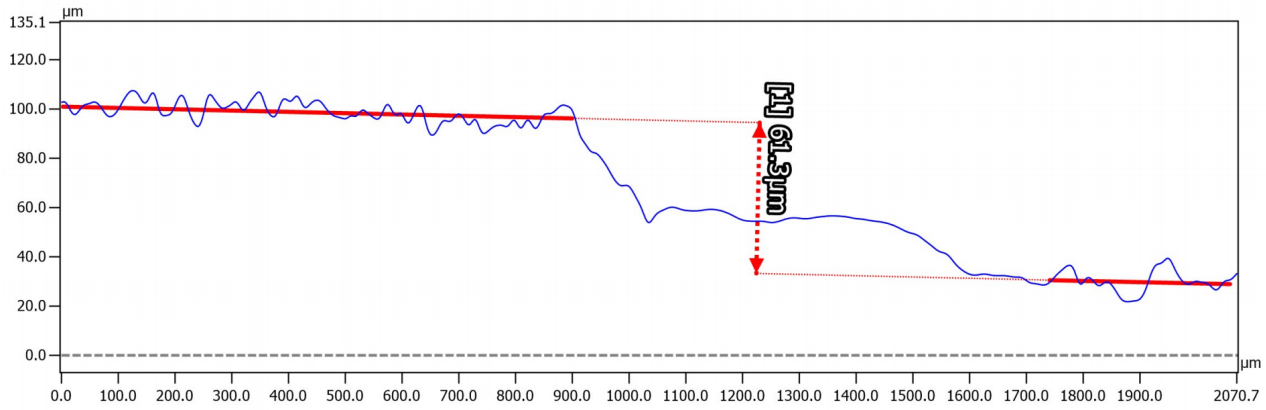

(b)

Figure 2.5: (a) Height surface image of the PNC coated on a PCB substrate in a 2 mm x 2 mm area. (b) Profile of the surface through the middle of the image shown in (a).

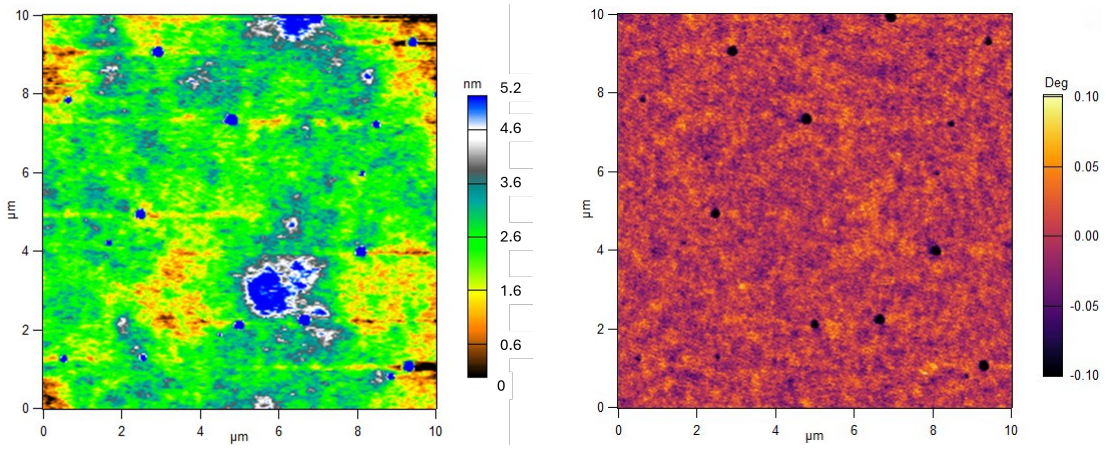

(a) (b)

Figure 2.6: (a) Topography of PNC. (b) NAP phase of PNC, dark dots show nanoparticle locations under 5 V bias.

Chapter 3

Effect of Conformal Coating on Electric Field Around PCB Electrode in Air: Simulation

The purpose of this chapter is to evaluate the effect of the PNC coating on the electric field distribution at critical TP regions in MV insulation structures. Finite element simulations were conducted to quantify the reduction in electric field intensity achieved by the nonlinear PNC coating relative to both uncoated and linearly coated surfaces.

All simulations were performed using COMSOL Multiphysics with the electric currents physics interface under AC 50 Hz conditions. The analysis was designed to replicate the local electric field environment at a conductor-dielectric-air interface, mimicking the layout discussing in chapter 4.

3.1 Simulation Setup

3.1.1 Geometry

The simulation domain represents a simplified two-dimensional cross section of a HV conductor edge, dielectric substrate, and surrounding air, as illustrated schematically in Fig.

3.1. The geometry dimensions were chosen to approximate the physical test structure used in PDIV and flashover experiments. The PCB cross-section has FR4 1.5 mm thick and 1 oz copper, approximately 35 μm thick. The HV trace has a 6 kV AC 50 Hz voltage applied. Similar to the cross-section measured, the PNC is designed to taper from the TP of the copper trace and is made to be about 60 μm thick near to the edge of the conductor.

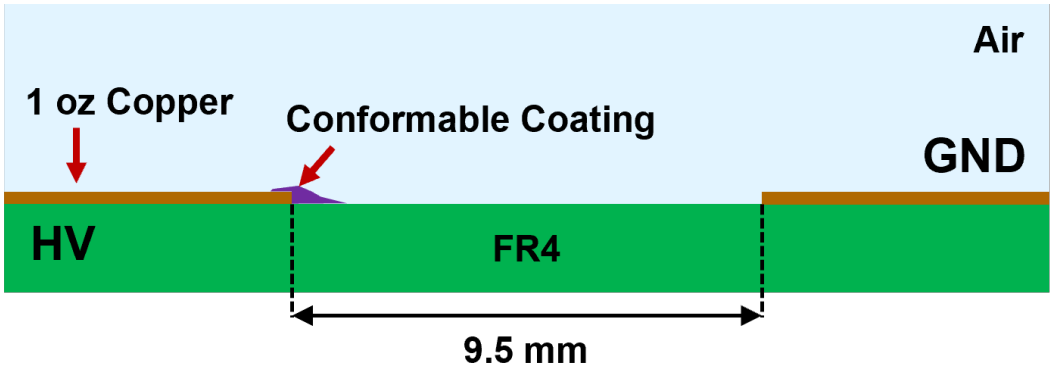

Figure 3.1: Geometry of the E-field simulation with a 9.5 mm gap between the HV and GND traces.

3.1.2 Materials

Material properties used in the simulation are summarized in Table 3.1. Copper was modeled as a perfect conductor, while FR4 and air were treated as linear dielectrics with constant permittivities.

Table 3.1: Materials properties used in E-field simulation.

Material	Conductivity (S/m)	Relative permittivity
Copper	5.96e7	1
Air	1e-12	1.000589
FR4	1e-14	4.5
MG Coating	1e-13	3
PNC	$\delta_0 \left(1 + \left(\frac{E}{E_b}\right)^{\alpha}\right)$	3

The commercial conformal coating was represented by a homogeneous insulating layer with conductivity of 1e-13 S/m. The PNC coating was modeled using a field-dependent conductivity function to capture its nonlinear resistive behavior observed experimentally in [16]. The relation between conductivity δ and the local electric field intensity was defined as

$$\delta(E) = \delta_0 \left(1 + \left(\frac{E}{E_b}\right)^{\alpha}\right), \tag{3.1}$$

where δ_0 is the initial conductivity; E_b is the switching field; and α is the nonlinear coefficient. Table 3.2 lists the values of each of these variables.

Table 3.2: Values used in Equation 3.1.

Variable	Value
δ_0	1e-11 S/m
E_b	15 kV/mm
α	7

3.2 Results and Discussion

Fig. 3.2 shows the simulated electric field distribution for the uncoated configuration where the region in white around the edge of the electrode is E-field stress above the scale of the image. The profile of the coating is seen in this image but is placed to keep consistency in the mesh between all simulations. In the uncoated interface, strong field intensification occurs at the conductor-FR4-air triple point, with a peak field magnitude of 3.8 kV/mm 10 μm above surface of the FR4. This concentrated stress is above the dielectric strength of air (3 kV/mm) and this region correlates closely with the initiation site of partial discharge observed experimentally in subsection 4.2.

Application of the commercial conformal coating instead enhanced the maximum electric

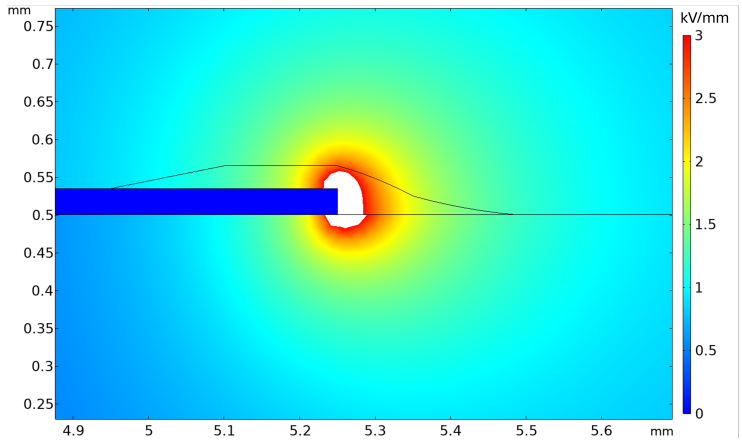

Figure 3.2: FEA simulation results with TP surrounded by air.

field to 10.2 kV/mm, shown in Fig. 3.3. This enhanced electric field may be attributed to the decrease in conductivity compared to air and However, the high E-field had been mostly contained within the coating material. Instead, a small location near the coating edge remained above the dielectric strength of air, continuing to be a point susceptible to PD and breakdown.

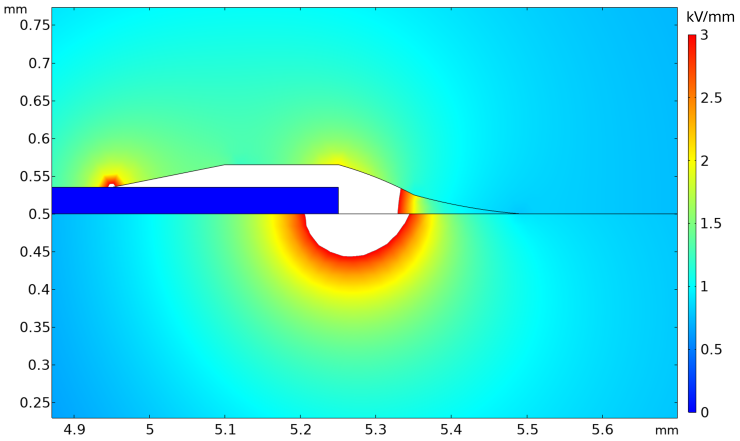

Figure 3.3: FEA simulation results with TP surrounded by the commercial MG material.

In contrast, the PNC-coated interface exhibited a significantly more uniform field distribution seen in Fig. 3.4. The peak field was reduced to approximately 2.5 kV/mm, corresponding to nearly a 50% reduction relative to the uncoated case. The nonlinear conductivity

of the PNC allowed for controlled charge transport within the coating, dynamically redistributing potential near the triple point and flattening the local field gradient.

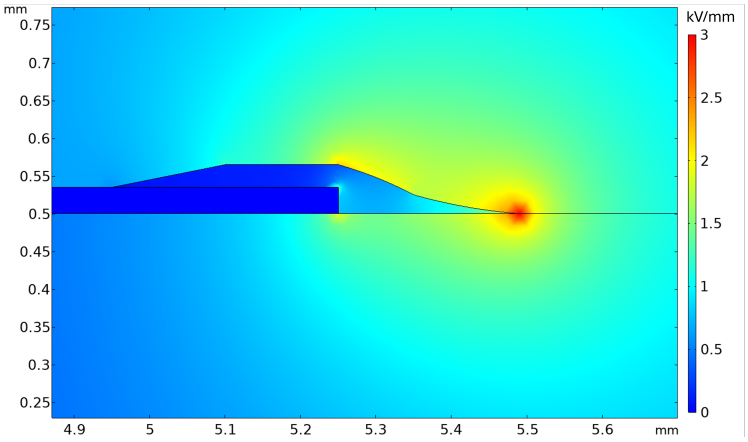

Figure 3.4: FEA simulation results with TP surrounded by air.

Fig. 3.5 compares the electric field profiles along the air–dielectric interface for the three cases 10 μm above the FR4 surface. The PNC-coated configuration exhibits the smoothest potential gradient and the lowest field enhancement factor, consistent with its experimentally observed suppression of PDIV activity and increase in flashover voltage seen in chapter 4.

3.3 Conclusion

Finite element electric field simulations were conducted to evaluate the field-grading effectiveness of the nonlinear polymer nanocomposite (PNC) coating at conductor–dielectric–air interfaces.

The PNC coating reduced the local electric field intensity at the triple point by approximately 50% compared to the uncoated configuration. The commercial linear coating instead showed enhancement of the field near the TP, but contained most of this stress within the material.

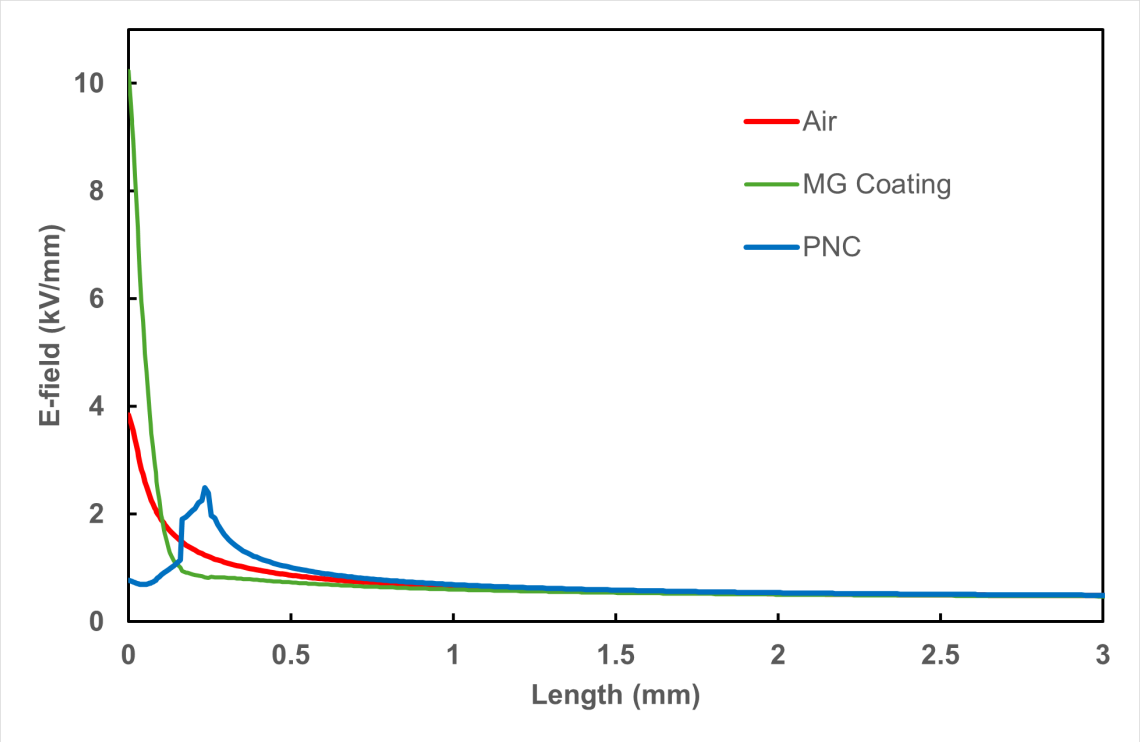

Figure 3.5: FEA simulation results with TP surrounded by air collected in a line 10 μm above the FR4.

These results confirm that the PNC's nonlinear conductivity enables smoothening of the E-field stress mitigation while applied in an air exposed environment. Consequently, the PNC coating is a promising field-grading solution for medium-voltage systems exposed to air.

Chapter 4

PNC Enhanced Flashover Voltage of PCBs at High Elevation

In medium-voltage (MV) power electronics, maintaining reliable surface insulation is critical to prevent partial discharge (PD) and flashover along air-exposed interfaces [21]. Many methods to suppress surface flashover have been developed in the last 50 years, ranging from electron beam irradiation [46], fluorination [47], plasma deposition [48, 49], and nonlinear conductivity coatings [31, 50–55]. The development of nonlinear resistive polymer nanocomposite (PNC) coatings provides a promising approach to mitigate these issues. By incorporating conductive nanoparticles into a polymer matrix, the coating exhibits field-dependent resistivity, enabling it to redistribute charge and locally suppress field intensification. To assess the coating's effectiveness, this chapter presents the results of PDIV and surface flashover BV testing under ambient environments and BV testing under low-pressure conditions that simulate high-altitude environments.

4.1 Experimental Setup

4.1.1 Sample Preparation

Printed circuit board (PCB) substrates made from FR4 were chosen for their widespread use in power electronics. The substrates were patterned with high-voltage copper electrodes designed to create distinct TP regions, where the conductor, insulating material, and air meet. Prior to coating, substrates were cleaned using ethanol to ensure optimal adhesion and minimal contamination to dust. Two types of coatings were utilized for comparison: a commercial conformal coating and the PNC coating. The commercial coating was formulated by MG Chemicals and is their 4226A clear insulating varnish, applied via brush. The PNC coating is formulated by incorporating semiconductive nanoparticles dispersed in a polymer matrix, also applied via brush and heat cured. Fig. 4.1 shows the PCB sample schematic and where the coatings are applied.

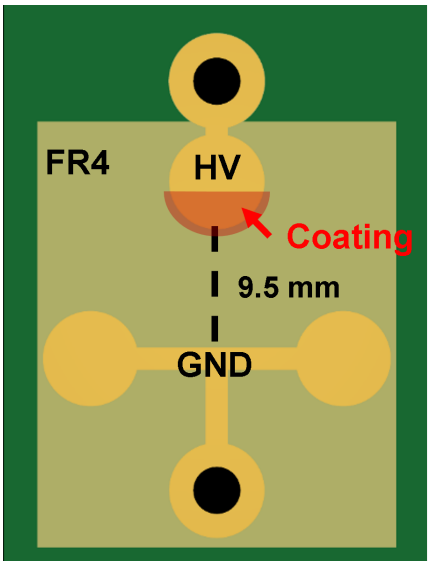

Figure 4.1: PCB sample schematic with a 9.5 mm gap between the HV and GND electrodes.

4.1.2 PDIV and Flashover Voltage Measurement Setup

To validate the effectiveness of the PNC coating in suppressing surface discharge and improving dielectric endurance, partial discharge inception voltage (PDIV) and surface flashover breakdown voltage (BV) tests were conducted under ambient atmospheric conditions. These measurements were designed to assess the onset of discharge activity and the ultimate dielectric failure point for PCB test structures with uncoated electrodes, commercially coated electrodes, and those coated with the nonlinear resistive PNC material.

A high-voltage AC power supply was used to apply a step-up voltage to each sample. The voltage ramping process was controlled to prevent sudden surges and to allow for monitoring of the PDIV and BV. The detection of partial discharges followed IEC 60270 guidelines, with a PD threshold set at 10 pC. A dedicated PD sensor and detection system recorded the voltage at which continuous discharges occurred over a 10-second interval, marking the PDIV. Fig. 4.2 shows the measurement setup as well as the circuit schematic.

4.1.3 Low-Pressure Flashover Voltage Measurement

To replicate high-altitude conditions, the coated and uncoated samples were placed inside a calibrated vacuum chamber. The chamber could achieve pressures corresponding to two different test altitudes: 50 kPa (∼5000 m altitude) and 20 kPa (∼10,000 m altitude). Pressure within the chamber was continuously monitored using a digital pressure gauge to ensure accurate simulation of the targeted environments. The same electrical setup used for PDIV testing is connected to this chamber for applying and monitoring partial discharge and breakdown. The chamber used to emulate high altitudes is pictured in Fig. 4.3.

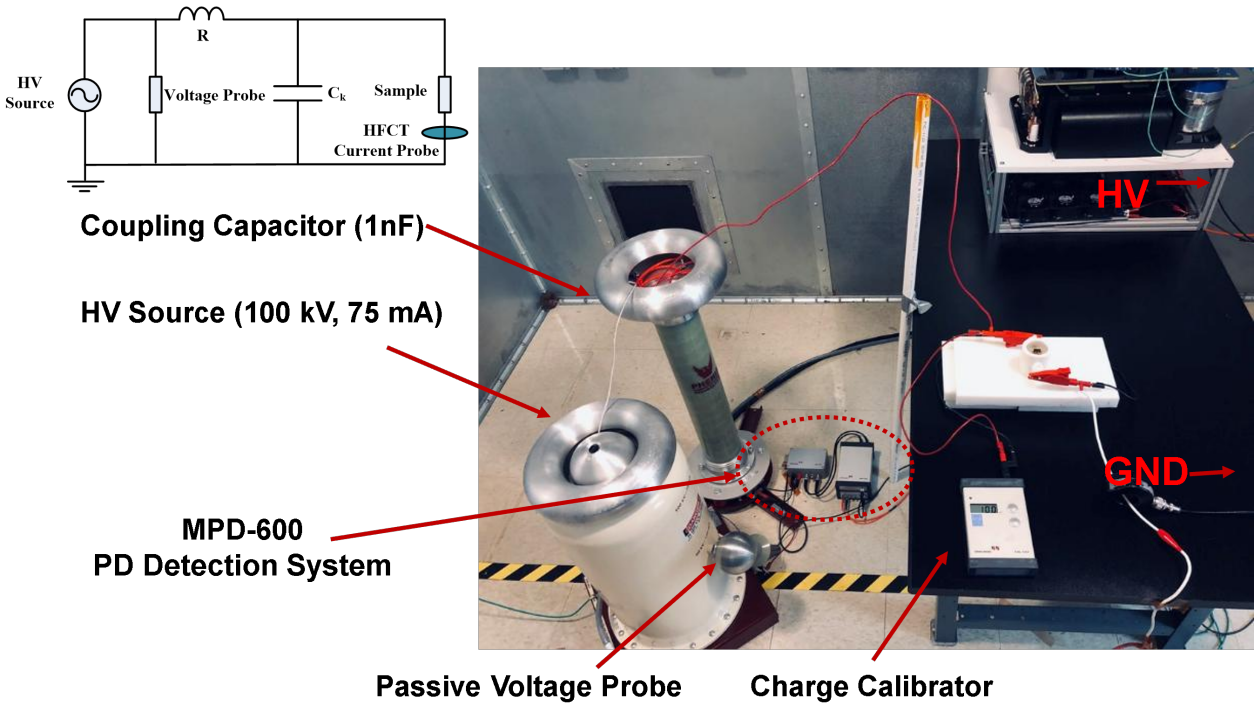

Figure 4.2: PDIV measurement setup with PD free HV source, coupling capacitor, MPD-600 detection system and sample under test. Circuit schematic is shown on the top left.

4.2 Results and Discussion

4.2.1 Ambient Air PDIV and BV Results

Fig. 4.4 shows the Weibull plot of the PDIV under ambient air conditions while Fig. 4.5 shows the Weibull plot of breakdown voltage as well as an image of its arc. Note that the flashover occurring in Fig. 4.5b connects with the circular electrode above the midpoint of the GND electrode. This may be attributed to a distorted electric field from imperfections in the manufacturing process or defects on the surface such as dust that make the arc favor a direction. Under 100 kPa pressure, the uncoated test samples exhibited partial discharge initiation at approximately 7.7 kV, followed shortly by complete surface flashover at 8.4 kV. This narrow gap between PDIV and breakdown suggests a high electric field concentration

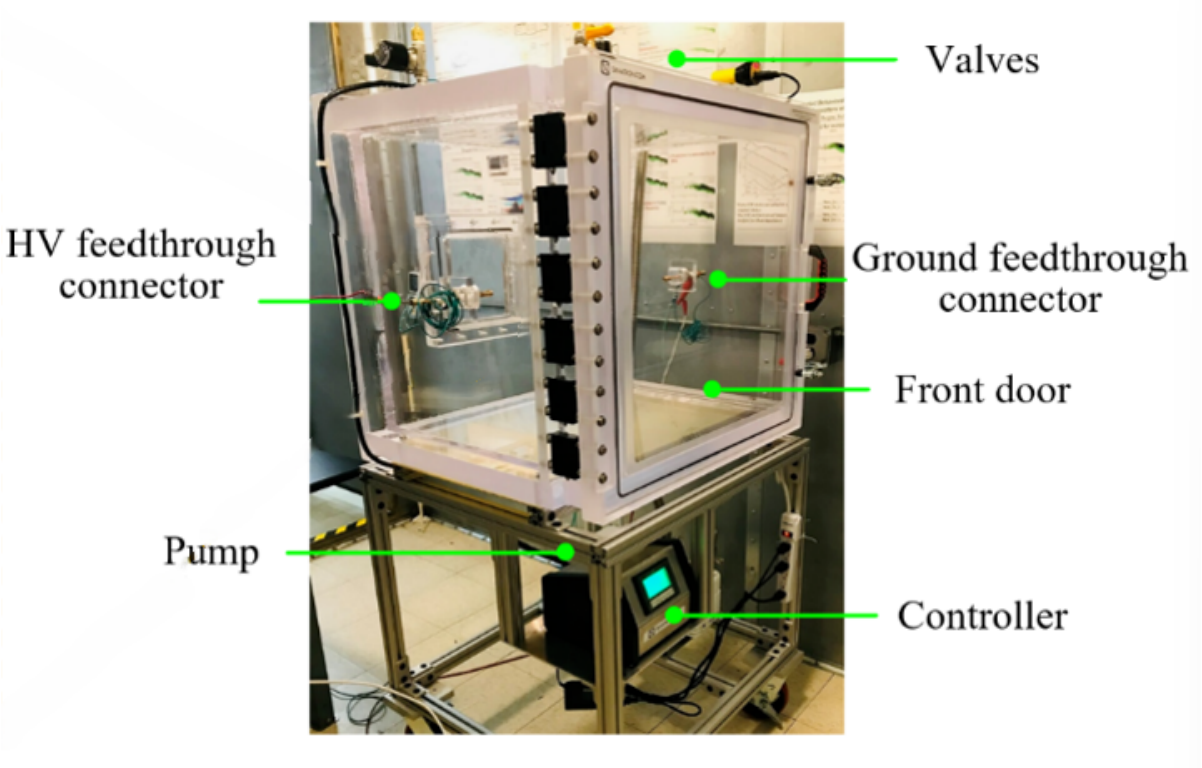

Figure 4.3: Acrylic vacuum chamber used to emulate high-altitude environments.

at the TP, leading to limited insulation margin and increased susceptibility to discharge propagation. After applying the MG coating, the PDIV increases to 8.3 kV and flashover voltage further increases to 9.1 kV. Samples coated with the commercial conformal coating showed a moderate improvement: PDIV was delayed beyond the uncoated threshold, and the breakdown voltage increased by more than 1 kV, suggesting that the linear dielectric layer provided some degree of field smoothing and charge suppression. In contrast to both of these groups, the samples coated with the PNC material do not experience PDIV before breaking down at 10.3 kV.

The most significant performance was observed in the samples coated with the PNC. No detectable partial discharge activity occurred before complete surface flashover, even as the applied voltage exceeded 10 kV. The PNC-coated structures experienced a clear shift in

breakdown voltage, demonstrating approximately a 30% increase in surface flashover voltage compared to the uncoated baseline. The absence of measurable PDIV before breakdown suggests that the PNC coating effectively dissipated surface charges and mitigated local electric field intensification, likely through the nonlinear conduction mechanism.

These results strongly support the notion that the PNC does not merely act as a high-dielectric-strength barrier, but instead participates in dynamic field control. Unlike the commercial coating, which delays but does not eliminate the early discharge activity, the PNC appears to prevent the formation of pre-breakdown discharge altogether. This behavior is consistent with the simulation results, which showed complete suppression of peak electric field intensity at the TP when the PNC was applied.

4.2.2 Breakdown Voltage Testing in Reduced Pressures

To evaluate the performance of the polymer nanocomposite (PNC) coating in high-altitude operational environments, surface flashover breakdown voltage (BV) tests were conducted at sub-atmospheric pressures representative of elevated altitudes. The test conditions were selected to emulate air densities corresponding to altitudes of approximately 5,000 m (50 kPa) and 10,000 m (20 kPa). These reduced-pressure environments are known to exacerbate surface flashover phenomena due to reduced concentration of air molecules that increases the mean free path for discharge events [31]. Results for 50 kPa are seen on Fig. 4.6 and 20 kPa is seen on Fig. 4.7.

Across all low-pressure test conditions, neither the uncoated samples nor the coated samples exhibited partial discharge activity prior to flashover. Instead, each configuration transitioned directly to complete surface breakdown once the critical electric field was reached. For all samples, this breakdown threshold decreased substantially with decreasing

pressure, confirming the inverse relationship between air density and breakdown voltage in surface discharge events.

The application of the commercial conformal coating provided a measurable improvement in breakdown voltage across all pressures tested, although the performance enhancement was moderate and proportional to its ambient-pressure behavior. In contrast, the PNC-coated samples consistently achieved the highest breakdown voltages at every simulated altitude. Notably, the PNC coating maintained an approximate 30% improvement in flashover voltage relative to the uncoated baseline, even at the lowest pressure tested. This consistent performance gain suggests that the nonlinear resistive field-grading mechanism of the PNC is preserved under reduced air density conditions.

4.3 Conclusion

The surface flashover suppression and discharge mitigation capability of a polymer nanocomposite (PNC) coating were investigated under both ambient and low-pressure air environments to enhance the insulation of air-exposed regions in printed circuit boards and power converters. The results show that the PNC remains effective in improving the surface flashover voltage and eliminating partial discharge activity, even under reduced-pressure conditions representative of high-altitude operation.

Under ambient conditions, the PNC coating increased the flashover voltage by approximately 30% compared to the uncoated baseline, while preventing measurable discharge inception before breakdown. When tested at simulated altitudes up to 15,000 m, all samples exhibited lower breakdown voltages in accordance with Paschen's Law; however, the PNC maintained its performance advantage, consistently outperforming both the uncoated and commercially coated samples. This demonstrates that the nonlinear field-grading mechanism

of the PNC remains effective even when air density is reduced.

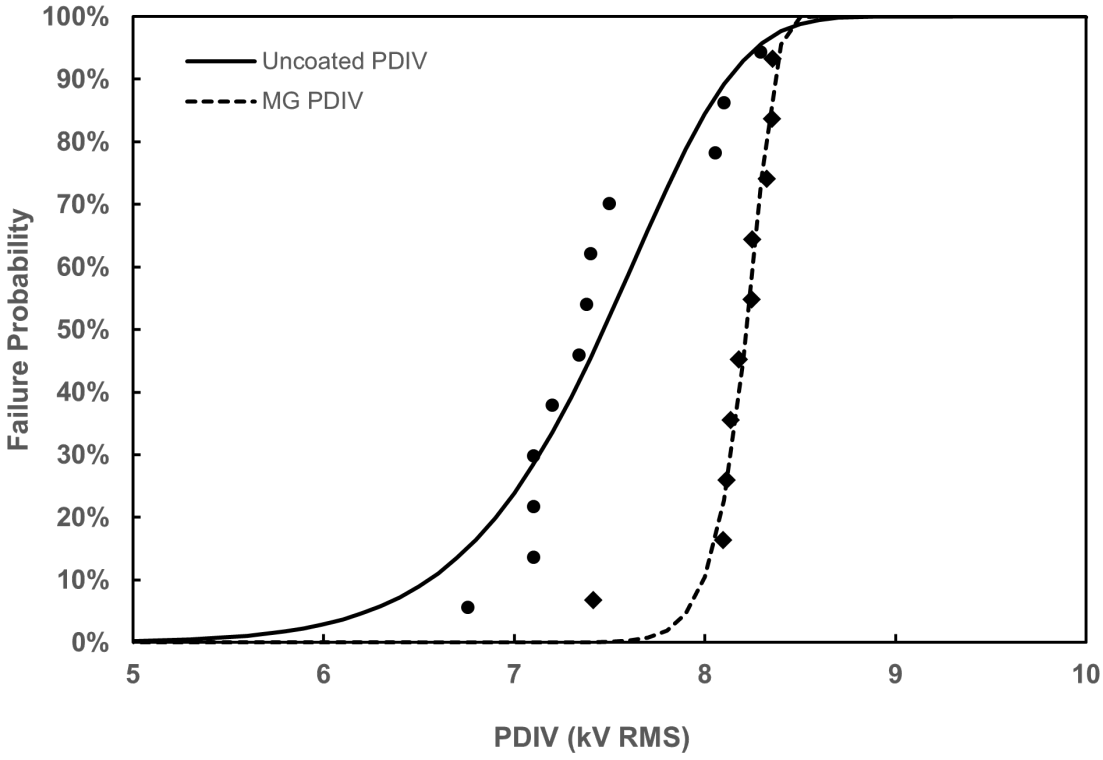

(a)

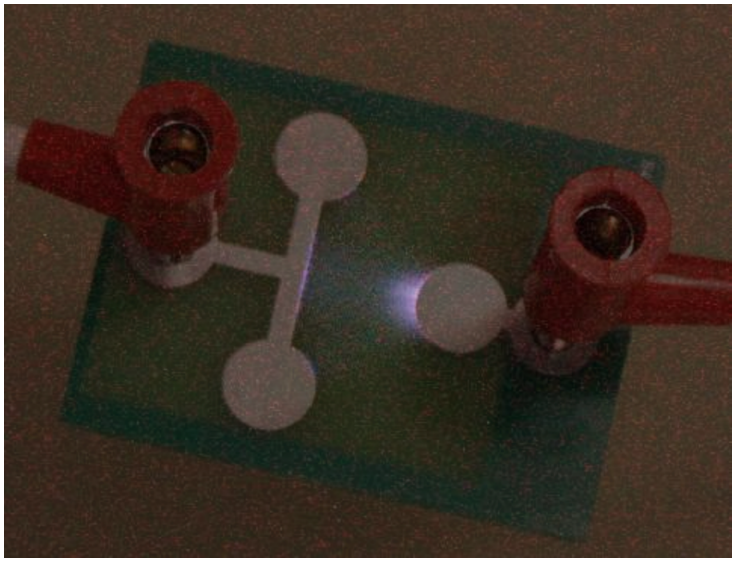

(b)

Figure 4.4: (a) PDIV results in ambient pressure. (b) Corona at the TP of the HV electrode.

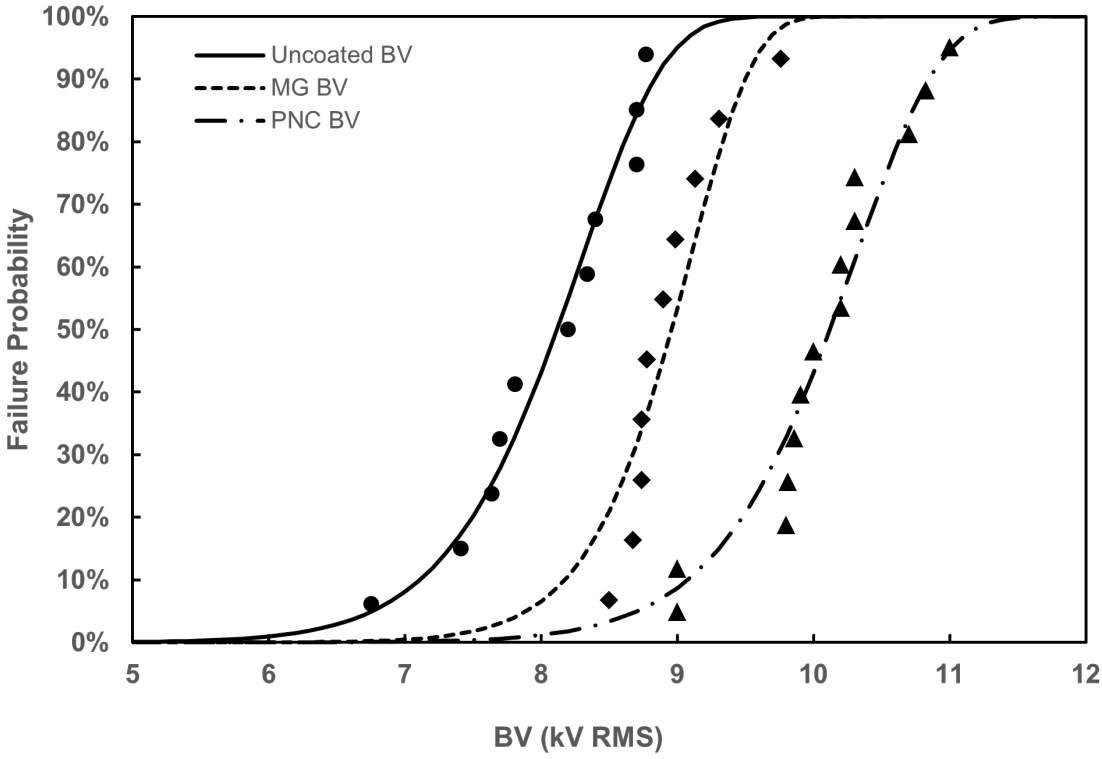

(a)

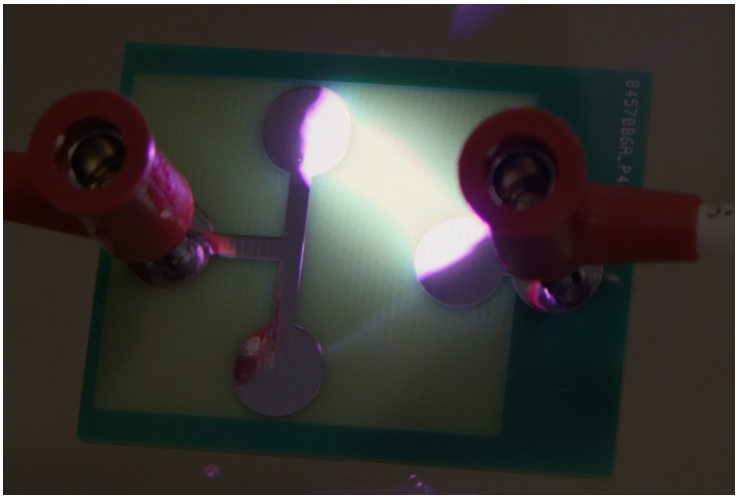

(b)

Figure 4.5: (a) BV results in ambient pressure. (b) Arc connecting the HV and GND electrodes.

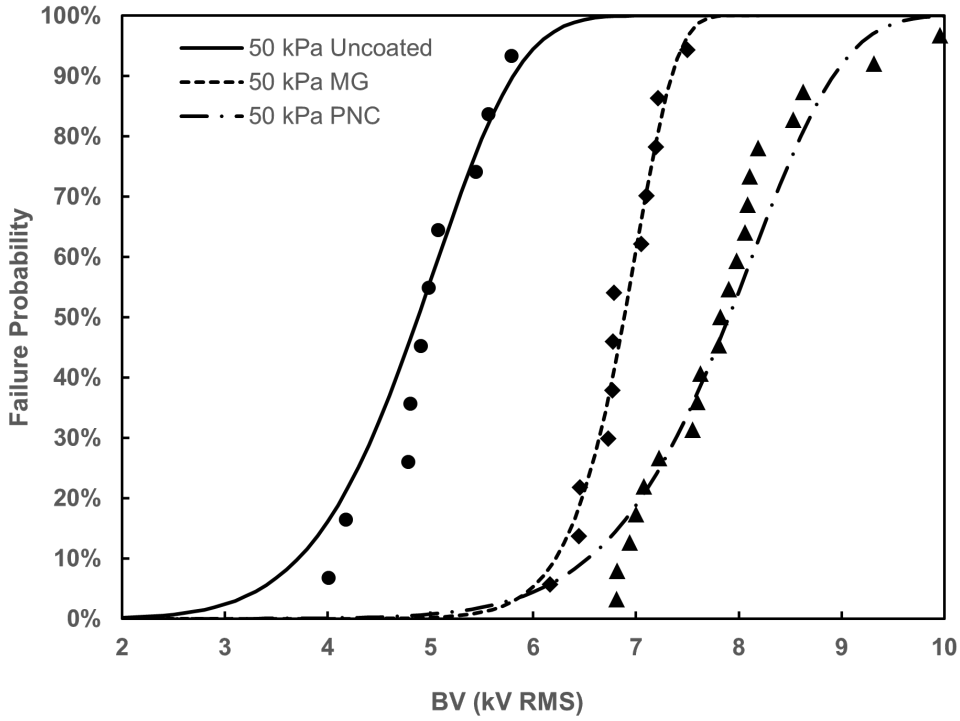

Figure 4.6: BV results in 50 kPa conditions within the vacuum chamber. Samples exhibit arc as seen in Fig. 4.5b.

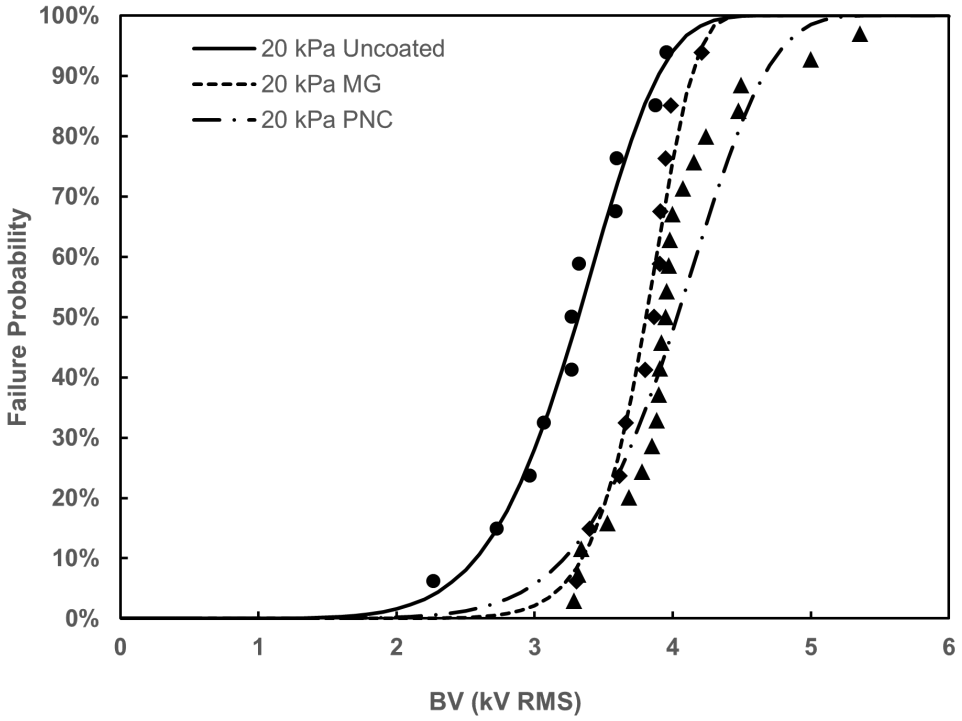

Figure 4.7: BV results in 20 kPa conditions within the vacuum chamber.

Chapter 5

Effect of Moisture on PNC Field-Grading in MV Power Modules

Moisture exposure is one of the most persistent reliability challenges for power modules, particularly when silicone-based encapsulants are used. Although silicone gels and elastomers provide good electrical insulation under dry conditions, they gradually absorb water vapor when placed in warm and humid environments [37]. Over time, this uptake can alter their electrical and mechanical properties, leading to reduced breakdown strength and increased leakage current [22, 35, 36]. Because the PNC field-grading coating is located at the triple point (TP), a region that already experiences intensified electric fields, its durability under humidity becomes critical for long-term module reliability. This chapter investigates the behavior of PNC-coated and uncoated alumina DBC substrates encapsulated in two silicone materials during controlled humidity aging and salt-fog exposure. The purpose is to determine whether the coating retains its ability to redistribute the electric field after moisture diffusion and whether environmental stressors introduce new degradation pathways that could reduce PDIV performance.

5.1 Experimental Setup

There are two common types of tests for power module reliability in humid conditions: high humidity, high temperature reverse bias (H^3TRB) [22], [56–63] and condensation tests [37], [64–68]. H^3TRB, also known as temperature, humidity, bias (THB) test, is a destructive test method that soaks the device under test (DUT) in constant conditions of 85°C, 85% relative humidity (RH), and as high a voltage as possible without significant self-heating from the power device and is generally used to prove the humidity robustness of power modules [57, 69]. The period the DUT is typically aged in this test condition is up to 1000 hours. Condensation tests involve immersing the DUT in less severe conditions such as 35°C, 70% RH while also cooling the DUT with a cooling element such as a heat sink or cold plate, inducing condensation within the encapsulant [37, 64, 65]. These tests are conducted over the course of 20-40 hours without placing the DUT under bias. These test methods are all used for determining the robustness of power modules and an increase of the power device leakage current is a typical failure condition. Another aging environment that would evaluate the robustness of the PNC material in an offshore environment is the salt fog method. This method can be used to evaluate the effects of salt deposits on the physical and electrical aspects of the material. The encapsulant insulation capability and how humidity impacts the PDIV is not typically measured. To measure how humidity and salinity influences the insulation performance of silicone gel, PDIV is a necessary measurement.

5.1.1 Mass Change Measurements of DBC Substrates

To evaluate the effectiveness of the coating after aging in a humid environment, samples of alumina DBC substrates were prepared according to the dimensions shown in Fig. 5.1a. The copper pattern on the substrate was chemically etched where a 2 mm trench gap is

typical in MV power modules. The PNC coating was applied to the TP of the high-voltage (HV) copper pad then encapsulated in a silicone gel pictured in Fig. 5.1b. Two silicone encapsulants were chosen to test: a soft silicone gel and a harder silicone elastomer. DBC samples are then placed in a chamber of ambient 70°C/70% RH conditions, aged for up to 500 hrs. The conditions of 70°C/70% RH were chosen after determining they are sufficient for moisture to intrude into the samples according to [37]. After aging in the chamber for 200/500 hrs, samples were then removed and weighed to test the mass change. The measurement would validate that the samples have experienced change after aging in this environment.

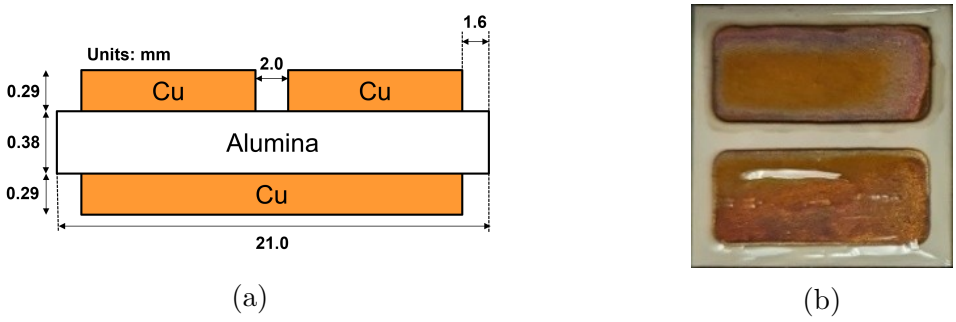

(a) (b)

Figure 5.1: (a) Schematic of alumina DBC test coupon. (b) Photo of a coated DBC substrate with silicone encapsulation

5.1.2 PDIV Measurements of DBC Substrates

After testing the mass change of the samples, the PDIV were measured immediately after. PDIV were tested by connecting the HV copper pad to a PD-free high-voltage 60 Hz ac source while the other top pad and bottom pad were grounded. The PD threshold level was set to 10 pC according to IEC 60270 with the PDIV being monitored by a PD detection system (MPD-600). Fig. 5.2 shows the PDIV measurement setup used in this study. PDIVs were recorded as the peak RMS voltage when PD levels exceed 10 pC continuously for 10

seconds.

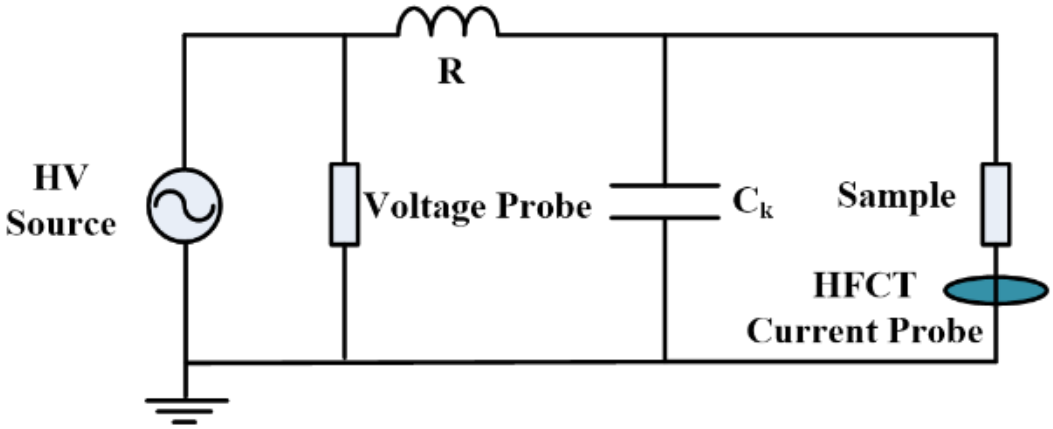

Figure 5.2: PDIV measurement setup with PD free HV source, coupling capacitor, MPD-600 detection system and sample under test.

5.1.3 Salt Fog Corrosion of Coated DBC Substrates

The same DBC samples pictured in Fig. 5.1 will also be used in this test. Samples will be exposed to conditions of 35°C and sprayed with a 5% sodium chloride solution as the salt spray, where the relative humidity would reach a maximum value of 100% during testing, as outlined in MIL-STD-810H. The test will be performed over the course of 72 hours, where the samples will experience wet and dry cycles of 24 hours. After samples experience these conditions, PDIV will be measured to evaluate the effectiveness of the PNC material as outlined in the previous section.

5.2 Results and Discussion

5.2.1 Mass Change Results

Fig. 5.3 shows the average mass change for each encapsulation type and aging times 200 and 500 hrs. The mass increased for all samples by a small amount indicating an intrusion of moisture into the silicone encapsulants. A small amount of mass loss is seen between the 200 and 500 hr aging times. This mass loss phenomenon is also seen in [22] as mass loss in 85°C/85% RH conditions. Above the glass transition temperature (T_g), which is less than -100°C for silicone gels and elastomers, the absorbed water breaks the bond between the fillers and the polymer chain [70]. This hydrothermal reaction causes a loss of material in the form of small particles and, consequently, a decrease in mass.

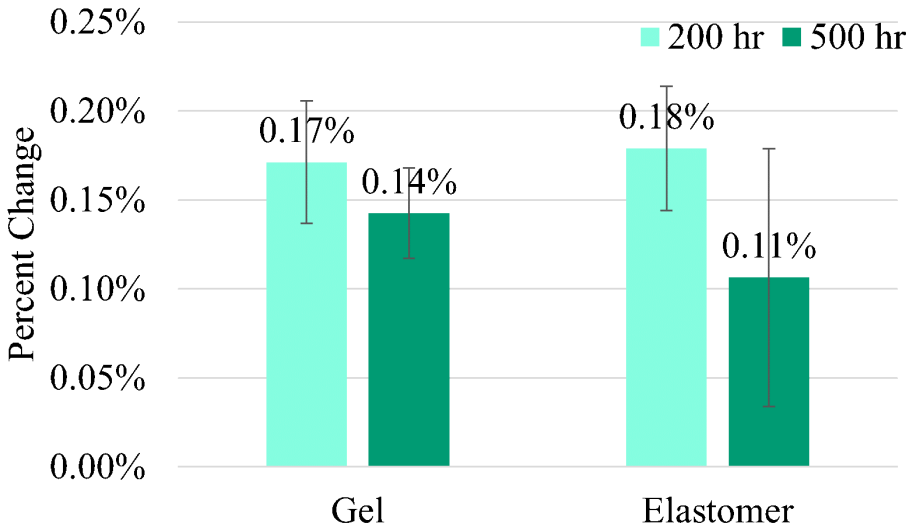

Figure 5.3: Average percent mass change for encapsulated DBC samples for 200/500 hr aging times.

5.2.2 PDIV Results

Fig. 5.4 shows the PDIV results of both silicone gel and elastomer encapsulated DBC substrates with and without the PNC coating applied. For both types of encapsulant, the PNC remains effective at increasing the PDIV of the encapsulated DBC substrates over the course of aging in a humid environment for 500 hrs. Even with moisture absorbed into the gels, the PNC continues to grade the E-field at the triple point in these DBC substrates. Fig. 5.5 shows the percent improvement to the PDIV from uncoated to coated DBC substrates. The percent improvement for silicone gel encapsulated samples show a relatively constant percent improvement over the course of 500 hrs, showing the effectiveness of the PNC material. For the silicone elastomer encapsulated samples, a decrease in the percent improvement is seen over the course of 500 hrs. This trend can be explained by the development of microcracks in the silicone elastomer. Microcracks would have been generated by the hydrothermal reaction discussed before and retained due to the greater modulus the elastomer has compared to the gel.

5.2.3 Salt Fog Corrosion PDIV Results

Fig. 5.6 shows the PDIV results of the elastomer encapsulated DBC samples with and without the PNC coating applied before and after the salt fog aging. After enduring salt fog conditions, the samples all saw a decrease in PDIV. Uncoated samples encountered a much lower decrease than those coated with PNC coating. A potential explanation for this phenomenon is the ingression of sodium and chlorine ions to the PNC coating would cause an increase in the conductivity of the coating due to an increase in electron carriers. This increase in conductivity would then cause the PNC to have reduced effectiveness in grading the electric field.

5.3 Conclusion

The field-grading effectiveness and reliability of a polymer nanocomposite coating were studied under humid conditions for improving the electrical insulation of a silicone gel or a silicone elastomer encapsulated medium-voltage power modules. The results show that the PNC remains effective in improving the partial discharge inception voltage of medium-voltage power modules, even after prolonged exposure to a 70°C/70% RH environment. The mass change results confirm that moisture intrusion occurred within the silicone encapsulants, leading to small mass losses over time due to hydrothermal degradation. However, despite the moisture uptake, the PNC coating consistently enhanced the PDIV of silicone gel-encapsulated modules, with minimal reduction in performance after 500 hours of aging. For the silicone elastomer-encapsulated samples, the performance of the PNC degraded more over time, likely due to the formation of microcracks caused by the hydrothermal reaction and the elastomer's higher elastic modulus. Overall, the PNC showed its promise for improving electrical insulation of MV power modules under humid conditions. Further research is needed to explore the PNC's robustness in other extreme conditions such as in a low-pressure environment for aerospace applications and verify the hypothesis of an increase in conductivity of the PNC after salt fog aging.

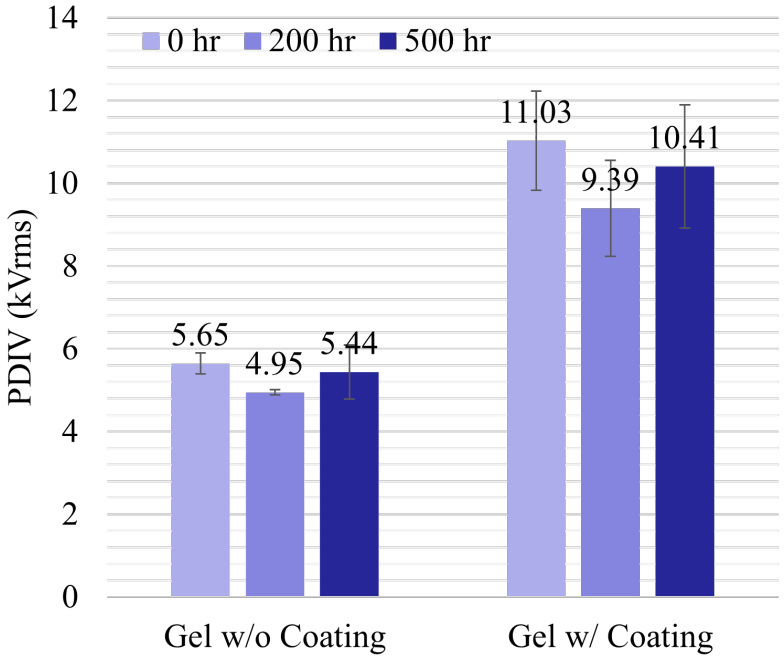

(a)

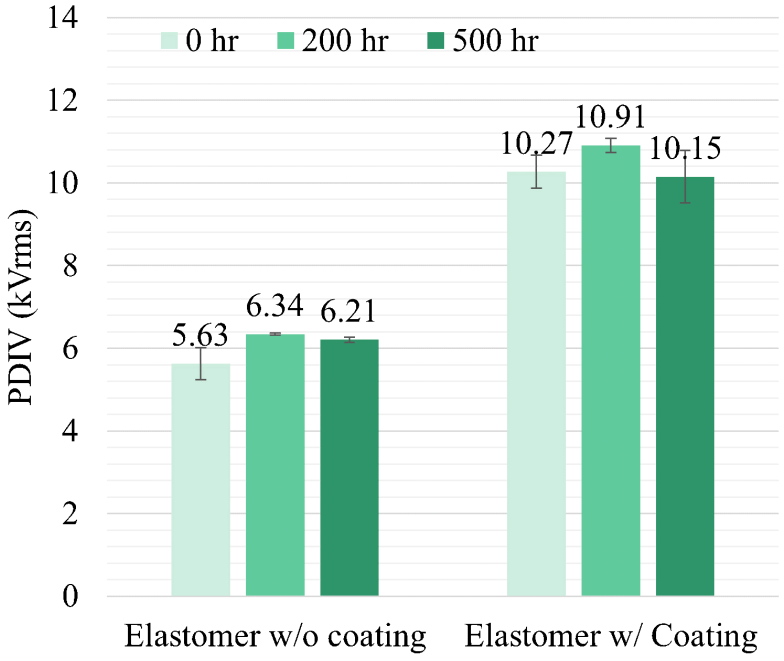

(b)

Figure 5.4: Average PDIV for both gel (a) and elastomer (b) encapsulated gel DBC samples for 200/500 hr aging times.

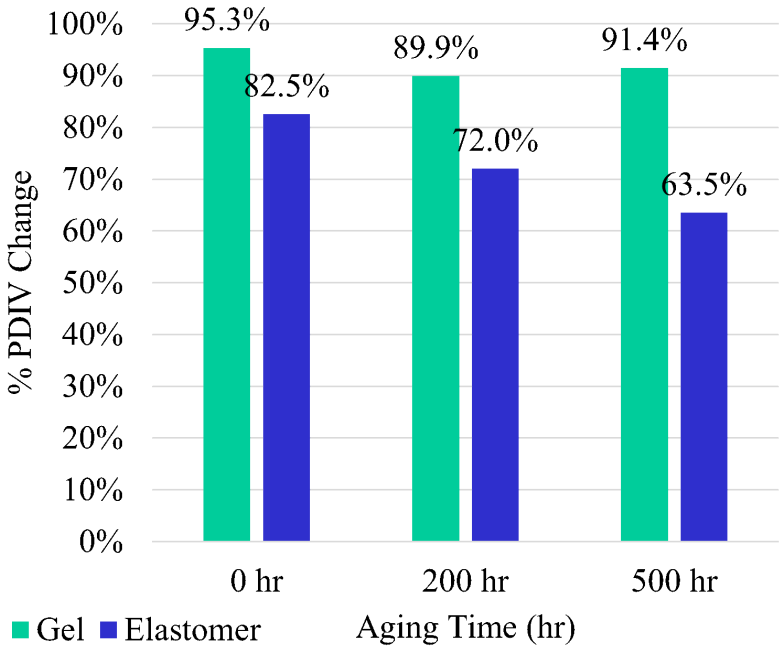

Figure 5.5: Percent improvement of PDIV from uncoated to coated DBC substrates for each encapsulation material and aging time.

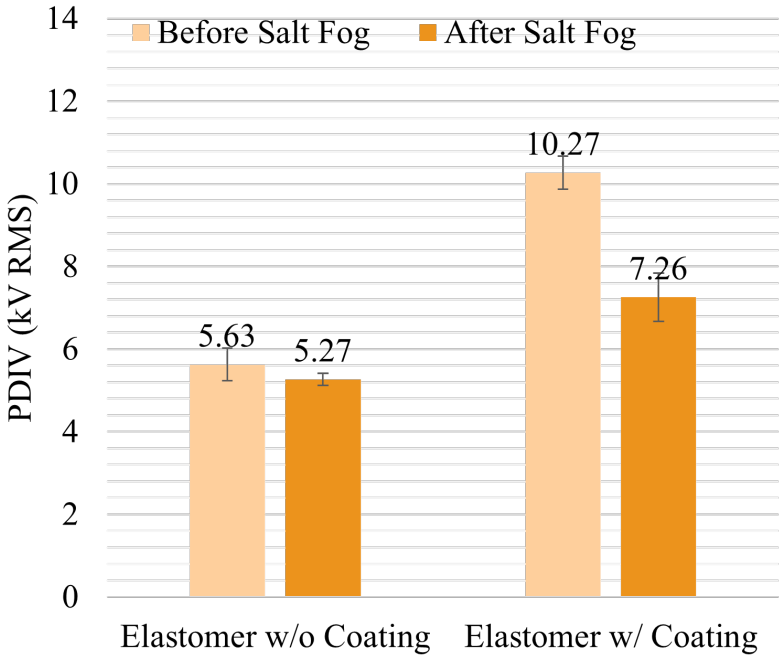

Figure 5.6: Average PDIV for elastomer encapsulated gel DBC samples before and after salt fog aging.

Chapter 6

Summary

The electrification of transportation, renewable energy, and aerospace applications has increased the need for reliable MV insulation systems capable of operating under elevated electrical, thermal, and environmental stress. WBG semiconductors, such as SiC and GaN, have enabled higher switching frequencies and voltages but have also intensified electric field stresses within power module encapsulants and at air-exposed interfaces. These stresses are particularly severe at TPs, where conductor, dielectric, and air interfaces converge. At such locations, the E-field can lead to PD or even breakdown of the insulation materials.

This research investigated a PNC coating designed as a nonlinear field-grading material for mitigating electric field intensification in MV insulation systems. The PNC, consisting of a polymer matrix with dispersed conductive nanoparticles, offers field-dependent conductivity that redistributes local stress without compromising insulation integrity. Through a combination of materials characterization, finite element simulation, and experimental validation, this thesis evaluated the effectiveness of the PNC under a range of environmental conditions representative of terrestrial and aerospace applications.

6.1 Material Characterization and Morphology

Chapter 2 examined the morphology and nanoparticle distribution of the PNC coating. SEM and EFM confirmed a uniform nanoparticle dispersion with no observable voids or

aggregation, ensuring homogeneity in electrical response. Surface morphology analysis using profilometry and AFM revealed a smooth and continuous coating with sub-nanometer surface roughness, suitable for conformal coverage on PCB substrates and power module electrodes.

The combination of uniform morphology and nanoscale particle distribution enables the coating to maintain stable dielectric interfaces. These results establish a strong foundation for the PNC's use as a conformal field-grading material compatible with standard power module fabrication processes.

6.2 Electric Field Simulation of Triple Points

Chapter 3 used finite element modeling to quantify the field-suppression effect of the PNC at TP regions under AC conditions. Simulations of uncoated, commercially coated, and PNC coated geometries demonstrated that the PNC significantly reduces local electric field peaks through nonlinear conduction.

The uncoated TP exhibited maximum field intensities exceeding 3.8 kV/mm, surpassing the dielectric strength of air. A commercial linear coating slightly reduced the field magnitude but contained much of the stress internally. In contrast, the PNC coating reduced peak field intensity by approximately 50% relative to the uncoated configuration and smoothed the potential distribution along the dielectric–air interface. These results confirm that the nonlinear resistivity of the PNC enables dynamic field redistribution, directly supporting the experimentally observed improvements in partial discharge inception and flashover voltage.

6.3 Surface Flashover and Low-Pressure Performance

Chapter 4 experimentally evaluated the PNC's insulation performance in air environments under both ambient and low-pressure conditions. PDIV and flashover breakdown voltage (BV) tests were conducted on PCB samples with uncoated, commercial, and PNC coated electrodes.

Under ambient pressure, the PNC increased the surface flashover voltage by approximately 30% compared to the uncoated baseline, with no measurable PD activity prior to breakdown. This result confirms the coating's ability to suppress pre-breakdown discharge through field grading rather than pure dielectric blocking.

When tested under reduced air pressures corresponding to altitudes up to 10,000 m, all samples exhibited lower absolute breakdown voltages consistent with Paschen's Law. However, the PNC maintained its relative performance advantage, preserving roughly a 30% improvement in flashover voltage compared to uncoated samples even at the lowest pressure tested. This consistency under reduced air density demonstrates that the nonlinear conduction mechanism remains functional in high-altitude environments, making the PNC a viable insulation enhancement for aerospace and high-altitude power systems.

6.4 Humidity Aging in Encapsulated Modules

Chapter 5 assessed the long-term reliability of the PNC in humid environments, where moisture absorption typically reduces the effectiveness of silicone encapsulants.

Mass change analysis confirmed moisture intrusion in both silicone gel and elastomer encapsulated DBC samples aged for up to 500 hours at 70°C/70% RH. Despite this, the PNC coating consistently increased PDIV relative to uncoated references throughout the aging

process. The PDIV improvement remained nearly constant for silicone gel encapsulated modules, while elastomer-encapsulated samples exhibited some reduction over time, likely due to microcrack formation from hydrothermal stress.

Additional salt fog testing revealed a decrease in PDIV for all samples, with a more pronounced effect for PNC-coated structures. This behavior may result from ionic contamination altering the conductivity of the coating. Nevertheless, the PNC remained functionally effective in grading the electric field, even after extended exposure to humid and corrosive conditions.

6.5 Overall Findings and Future Outlook

From the findings of this work, the polymer nanocomposite coating demonstrated consistent field-grading performance and robust environmental reliability.

These findings collectively demonstrate that the PNC coating effectively mitigates high-field stress at critical insulation interfaces, providing a material-based approach to enhance dielectric reliability in MV systems. Its nonlinear conduction behavior enables adaptive field control without requiring larger insulation distances or significant design modifications.

Future research should extend the evaluation of the PNC to long-term thermal cycling, high-frequency switching environments, and application to other high intensity E-field regions, such as device edge termination. Additionally, studying the effect of ionic contamination on PNC conductivity and exploring protective overcoats may further improve environmental robustness for aerospace and offshore applications. Investigation into changes of the surface morphology before and after humidity aging and salt fog corrosion could give insight into how the PNC changes, material or structural, under these conditions.

Overall, this work establishes the polymer nanocomposite coating as a promising field-grading solution for next-generation MV power modules, offering a path toward smaller, lighter, and more reliable insulation systems capable of withstanding both terrestrial and extreme environmental conditions.

Bibliography

[1] Shiqi Ji, Zheyu Zhang, and Fred Wang. "Overview of high voltage sic power semiconductor devices: development and application". In: *CES Transactions on Electrical Machines and Systems* 1.3 (Sept. 2017). Conference Name: CES Transactions on Electrical Machines and Systems, pp. 254–264. ISSN: 2096-3564. DOI: 10.23919/TEMS.2017.8086104. URL: https://ieeexplore.ieee.org/document/8086104 (visited on 10/14/2024).

[2] Marcin Hajlasz. "Gold free contacts to AlGaN/GaN heterostructures". English. In: (May 2018). DOI: 10.3990/1.9789036545389. URL: https://research.utwente.nl/en/publications/gold-free-contacts-to-algangan-heterostructures/ (visited on 10/30/2025).

[3] Yuliang Cao, Khai Ngo, and Dong Dong. "A Scalable Electronic-Embedded Transformer, a New Concept Toward Ultra-High-Frequency High-Power Transformer in DC–DC Converters". In: *IEEE Transactions on Power Electronics* 38.8 (Aug. 2023), pp. 9278–9293. ISSN: 1941-0107. DOI: 10.1109/TPEL.2023.3279259. URL: https://ieeexplore.ieee.org/document/10132061 (visited on 10/30/2025).

[4] Yuliang Cao et al. "Switching Transition Analysis and Optimization for Bidirectional CLLC Resonant DC Transformer". In: *IEEE Transactions on Power Electronics* 37.4 (Apr. 2022), pp. 3786–3800. ISSN: 1941-0107. DOI: 10.1109/TPEL.2021.3125265. URL: https://ieeexplore.ieee.org/document/9601280 (visited on 10/30/2025).

[5] Jian Liu et al. "12-kV 1-kA Breaking Capable Modular Power Electronic Interrupter With Staged Turn-off Strategy for Medium-Voltage DC Hybrid Circuit Breaker". In: *IEEE Transactions on Industry Applications* 58.5 (Sept. 2022), pp. 6343–6356. ISSN:

1939-9367. DOI: 10.1109/TIA.2022.3185570. URL: https://ieeexplore.ieee.org/document/9804794 (visited on 10/30/2025).

[6] Jian Liu, Di Zhang, and Dong Dong. "Analysis of Hybrid Modular Multilevel Rectifier Operated at Nonunity Power Factor for HVDC Applications". In: *IEEE Transactions on Power Electronics* 37.9 (Sept. 2022), pp. 10642–10657. ISSN: 1941-0107. DOI: 10.1109/TPEL.2022.3164099. URL: https://ieeexplore.ieee.org/document/9747999 (visited on 10/30/2025).

[7] Xiangchen Liu et al. "Characteristics and Identification of Partial Discharge for Insulation Structures in High Voltage IGBT Modules Under Positive Square Wave Voltage". In: *IEEE Transactions on Power Electronics* 38.4 (Apr. 2023). Conference Name: IEEE Transactions on Power Electronics, pp. 5347–5359. ISSN: 1941-0107. DOI: 10.1109/TPEL.2022.3232327. URL: https://ieeexplore.ieee.org/document/9999505 (visited on 08/28/2024).

[8] Jian Liu et al. "Compact MV-Insulated MHz Transformer-Coupled Gate Driver With Staged Turn-Off Scheme for Series-Connected Power Devices in DC Circuit Breaker Applications". In: *IEEE Journal of Emerging and Selected Topics in Power Electronics* 11.2 (Apr. 2023), pp. 1627–1638. ISSN: 2168-6785. DOI: 10.1109/JESTPE.2022.3227278. URL: https://ieeexplore.ieee.org/document/9973297 (visited on 10/30/2025).

[9] Xingchen Zhao et al. "Design of Ultracompact Gate Driver Integrated With Current Sensor and Commutation Path for a 211-kW Three-Level SiC Aircraft Propulsion Inverter". In: *IEEE Journal of Emerging and Selected Topics in Power Electronics* 11.4 (Aug. 2023), pp. 4077–4094. ISSN: 2168-6785. DOI: 10.1109/JESTPE.2023.3247378. URL: https://ieeexplore.ieee.org/document/10049466 (visited on 10/30/2025).

[10] Jiewen Hu et al. “Design and Qualification of a 100-kW Three-Phase SiC-Based Generator Rectifier Unit Rated for 50 000-Ft Altitude”. In: *IEEE Journal of Emerging and Selected Topics in Power Electronics* 11.2 (Apr. 2023), pp. 1865–1878. ISSN: 2168-6785. DOI: 10.1109/JESTPE.2022.3223415. URL: https://ieeexplore.ieee.org/document/9955519 (visited on 10/30/2025).

[11] Ripun Phukan et al. “Investigation of Staggered PWM Scheme for AC Common Mode Current Minimization in SiC-Based Three-Phase Inverters”. In: *IEEE Transactions on Transportation Electrification* 8.4 (Dec. 2022), pp. 4378–4390. ISSN: 2332-7782. DOI: 10.1109/TTE.2022.3198528. URL: https://ieeexplore.ieee.org/document/9855494 (visited on 10/30/2025).

[12] Ripun Phukan et al. “A Compact Integrated DM-CM Filter with PCB Embedded DC Current Sensor for High Altitude High Current Applications”. In: *2022 IEEE/AIAA Transportation Electrification Conference and Electric Aircraft Technologies Symposium (ITEC+EATS)*. ISSN: 2377-5483. June 2022, pp. 923–928. DOI: 10.1109/ITEC53557.2022.9814074. URL: https://ieeexplore.ieee.org/document/9814074 (visited on 10/30/2025).

[13] Zhao Yuan et al. “Design and Evaluation of A 150 kVA SiC MOSFET Based Three Level TNPC Phase-leg PEBB for Aircraft Motor Driving Application”. In: *2019 IEEE Energy Conversion Congress and Exposition (ECCE)*. ISSN: 2329-3748. Sept. 2019, pp. 6569–6574. DOI: 10.1109/ECCE.2019.8913071. URL: https://ieeexplore.ieee.org/abstract/document/8913071 (visited on 10/30/2025).

[14] Yuhang Yang et al. “Automotive Power Module Packaging: Current Status and Future Trends”. In: *IEEE Access* 8 (2020), pp. 160126–160144. ISSN: 2169-3536. DOI: 10.1109/ACCESS.2020.3019775. URL: https://ieeexplore.ieee.org/document/9178734 (visited on 10/30/2025).

[15] Gui-Jia Su et al. “A High-Power Density Segmented Traction Drive Inverter”. In: *2023 IEEE Energy Conversion Congress and Exposition (ECCE)*. ISSN: 2329-3748. Oct. 2023, pp. 1825–1830. DOI: 10.1109/ECCE53617.2023.10361985. URL: https://ieeexplore.ieee.org/document/10361985 (visited on 10/30/2025).

[16] Zichen Zhang, Khai D. T. Ngo, and Guo-Quan Lu. “Characterization of a Nonlinear Resistive Polymer-Nanoparticle Composite Coating for Electric Field Reduction in a Medium-Voltage Power Module”. In: *IEEE Transactions on Power Electronics* 37.3 (Mar. 2022). Conference Name: IEEE Transactions on Power Electronics, pp. 2475–2479. ISSN: 1941-0107. DOI: 10.1109/TPEL.2021.3112096. URL: https://ieeexplore.ieee.org/abstract/document/9536402 (visited on 10/20/2023).

[17] Zichen Zhang et al. “Packaging of an 8-kV Silicon Carbide Diode Module with Double-Side Cooling and Sintered-Silver Joints”. In: *2021 IEEE Electric Ship Technologies Symposium (ESTS)*. Aug. 2021, pp. 1–7. DOI: 10.1109/ESTS49166.2021.9512339. URL: https://ieeexplore.ieee.org/abstract/document/9512339 (visited on 10/20/2023).

[18] Zichen Zhang et al. “Evaluation of a Nonlinear Resistive Polymer-Nanoparticle Composite for Field-Grading in a Double-Side Cooled 10-kV Silicon Carbide Rectifier Module”. In: *CIPS 2022; 12th International Conference on Integrated Power Electronics Systems*. Mar. 2022, pp. 1–5. URL: https://ieeexplore.ieee.org/abstract/document/9861952 (visited on 10/20/2023).

[19] Boya Zhang, Mona Ghassemi, and Yunxiao Zhang. “Insulation Materials and Systems for Power Electronics Modules: A Review Identifying Challenges and Future Research Needs”. In: *IEEE Transactions on Dielectrics and Electrical Insulation* 28.1 (Feb. 2021). Conference Name: IEEE Transactions on Dielectrics and Electrical Insulation, pp. 290–

302. ISSN: 1558-4135. DOI: 10.1109/TDEI.2020.009041. URL: https://ieeexplore.ieee.org/document/9351883 (visited on 09/30/2024).

[20] Christina M. DiMarino et al. "10-kV SiC MOSFET Power Module With Reduced Common-Mode Noise and Electric Field". In: *IEEE Transactions on Power Electronics* 35.6 (June 2020). Conference Name: IEEE Transactions on Power Electronics, pp. 6050–6060. ISSN: 1941-0107. DOI: 10.1109/TPEL.2019.2952633. URL: https://ieeexplore.ieee.org/document/8894897 (visited on 10/07/2024).

[21] Lakshmi Ravi. "Insulation-Constrained Design of Power Electronics Converters and DC Circuit Breakers". en. In: (Nov. 2023). Publisher: Virginia Tech. URL: http://hdl.handle.net/10919/116664 (visited on 10/03/2024).

[22] Kaixuan Li et al. "Degradation behaviors of silicone gel encapsulation material with moisture intrusion". In: *Polymer Degradation and Stability* 206 (2022). Publisher: Elsevier Ltd. ISSN: 01413910. DOI: 10.1016/j.polymdegradstab.2022.110197.

[23] Nicholas M. Jordan et al. "Electric field and electron orbits near a triple point". In: *Journal of Applied Physics* 102.3 (Aug. 2007), p. 033301. ISSN: 0021-8979. DOI: 10.1063/1.2764211. URL: https://doi.org/10.1063/1.2764211 (visited on 09/30/2024).

[24] T. M. Do, J.-l. Auge, and O. Lesaint. "A Study of Parameters Influencing Streamer Inception in Silicone Gel". In: *IEEE Transactions on Dielectrics and Electrical Insulation* 16.3 (June 2009), pp. 893–899. ISSN: 1558-4135. DOI: 10.1109/TDEI.2009.5128532. URL: https://ieeexplore.ieee.org/document/5128532 (visited on 10/30/2025).

[25] Yalin Wang et al. "Space-Charge Accumulation and Its Impact on High-Voltage Power Module Partial Discharge Under DC and PWM Waves: Testing and Modeling". In: *IEEE Transactions on Power Electronics* 36.10 (Oct. 2021), pp. 11097–11108. ISSN: 1941-0107. DOI: 10.1109/TPEL.2021.3072655. URL: https://ieeexplore.ieee.org/document/9403933 (visited on 10/30/2025).

[26] J.-H. Fabian, S. Hartmann, and A. Hamidi. "Analysis of insulation failure modes in high power IGBT modules". In: *Fourtieth IAS Annual Meeting. Conference Record of the 2005 Industry Applications Conference, 2005.* Vol. 2. ISSN: 0197-2618. Oct. 2005, 799–805 Vol. 2. DOI: 10.1109/IAS.2005.1518425. URL: https://ieeexplore.ieee.org/document/1518425 (visited on 10/30/2025).

[27] Hugo Reynes, Cyril Buttay, and Hervé Morel. "Protruding ceramic substrates for high voltage packaging of wide bandgap semiconductors". In: *2017 IEEE 5th Workshop on Wide Bandgap Power Devices and Applications (WiPDA)*. Oct. 2017, pp. 404–410. DOI: 10.1109/WiPDA.2017.8170581. URL: https://ieeexplore.ieee.org/document/8170581 (visited on 10/30/2025).

[28] Hélène Hourdequin et al. "Metallized ceramic substrate with mesa structure for voltage ramp-up of power modules". en. In: *The European Physical Journal Applied Physics* 87.2 (Aug. 2019). Number: 2 Publisher: EDP Sciences, p. 20903. ISSN: 1286-0042, 1286-0050. DOI: 10.1051/epjap/2019180288. URL: https://www.epjap.org/articles/epjap/abs/2019/08/ap180288/ap180288.html (visited on 10/07/2024).

[29] Christoph Friedrich Bayer et al. "Partial discharges in ceramic substrates - correlation of electric field strength simulations with phase resolved partial discharge measurements". In: *2016 International Conference on Electronics Packaging (ICEP)*. Apr. 2016, pp. 530–535. DOI: 10.1109/ICEP.2016.7486884. URL: https://ieeexplore.ieee.org/document/7486884 (visited on 10/31/2025).

[30] Christoph Friedrich Bayer et al. "Stacking of Insulating Substrates and a Field Plate to Increase the PDIV for High Voltage Power Modules". In: *2016 IEEE 66th Electronic Components and Technology Conference (ECTC)*. May 2016, pp. 1172–1178. DOI: 10.1109/ECTC.2016.40. URL: https://ieeexplore.ieee.org/document/7545573 (visited on 10/31/2025).

[31] Shengtao Li et al. “Synergic effect of adsorbed gas and charging on surface flashover”. en. In: *Scientific Reports* 9.1 (Apr. 2019). Publisher: Nature Publishing Group, p. 5464. ISSN: 2045-2322. DOI: 10.1038/s41598-019-41961-0. URL: https://www.nature.com/articles/s41598-019-41961-0 (visited on 12/11/2024).

[32] Craig Hillman, Robert Esser, and Jim McLeish. *Failure mechanisms in high voltage printed circuit boards*. 2007. URL: https://www.circuitnet.com/news/uploads/1/Failure_Mechanisms_in_High_Voltage_PCBs.pdf.

[33] I Christou et al. “Choice of optimal voltage for more electric aircraft wiring systems | IET Electrical Systems in Transportation”. In: *IET Electrical Systems in Transportation* 1.1 (Mar. 2011), pp. 24–30. DOI: 10.1049/iet-est.2010.0021. URL: https://digital-library.theiet.org/doi/abs/10.1049/iet-est.2010.0021 (visited on 10/31/2025).

[34] Zhen Li et al. “Surface flashover in 50 years: Theoretical models and competing mechanisms”. en. In: *High Voltage* 8.5 (2023). _eprint: https://onlinelibrary.wiley.com/doi/pdf/10.1049/hve pp. 853–877. ISSN: 2397-7264. DOI: 10.1049/hve2.12340. URL: https://onlinelibrary.wiley.com/doi/abs/10.1049/hve2.12340 (visited on 12/02/2024).

[35] M. Sherriff et al. “Investigation of the impact of temperature and humidity on the capacitance of dielectric gel used for power electronics”. In: *11th International Conference on Power Electronics, Machines and Drives (PEMD 2022)*. Vol. 2022. June 2022, pp. 91–96. DOI: 10.1049/icp.2022.1023. URL: https://ieeexplore.ieee.org/document/9868534 (visited on 10/28/2023).

[36] Mark Sherriff et al. “Partial Discharge in Silicone Gel on Power Module Substrates in High-Humidity Conditions”. In: *IEEE Transactions on Dielectrics and Electrical Insulation* (2024). Conference Name: IEEE Transactions on Dielectrics and Electrical

Insulation, pp. 1–1. ISSN: 1558-4135. DOI: 10.1109/TDEI.2024.3404367. URL: https://ieeexplore.ieee.org/document/10536112 (visited on 09/10/2024).

[37] Kenji Hatori et al. "Humidity Absorption Behavior of Silicone Gel in HVIGBT Modules". In: *2021 23rd European Conference on Power Electronics and Applications (EPE'21 ECCE Europe)*. Sept. 2021, P.1–P.8. DOI: 10.23919/EPE21ECCEEurope50061.2021.9570514. URL: https://ieeexplore.ieee.org/document/9570514 (visited on 10/30/2023).

[38] L. Donzel and J. Schuderer. "Nonlinear resistive electric field control for power electronic modules". In: *IEEE Transactions on Dielectrics and Electrical Insulation* 19.3 (June 2012). Conference Name: IEEE Transactions on Dielectrics and Electrical Insulation, pp. 955–959. ISSN: 1558-4135. DOI: 10.1109/TDEI.2012.6215099. URL: https://ieeexplore.ieee.org/document/6215099/?arnumber=6215099 (visited on 08/05/2024).

[39] Kaixuan Li et al. "Electric Field Mitigation in High-Voltage High-Power IGBT Modules Using Nonlinear Conductivity Composites". In: *IEEE Transactions on Components, Packaging and Manufacturing Technology* 11.11 (Nov. 2021). Conference Name: IEEE Transactions on Components, Packaging and Manufacturing Technology, pp. 1844–1855. ISSN: 2156-3985. DOI: 10.1109/TCPMT.2021.3106962. URL: https://ieeexplore.ieee.org/document/9521194/?arnumber=9521194 (visited on 08/05/2024).

[40] Yuan Gao et al. "Analysis of Nonlinear Conductivity Coating used to Improve Electric Field Distribution in Medium Voltage Power Module". In: *2022 IEEE Energy Conversion Congress and Exposition (ECCE)*. ISSN: 2329-3748. Oct. 2022, pp. 1–7. DOI: 10.1109/ECCE50734.2022.9947302. URL: https://ieeexplore.ieee.org/document/9947302/?arnumber=9947302 (visited on 08/05/2024).

[41] Xiao Yang et al. “Grading electric field in high voltage insulation using composite materials”. In: *IEEE Electrical Insulation Magazine* 34.1 (Jan. 2018). Conference Name: IEEE Electrical Insulation Magazine, pp. 15–25. ISSN: 1558-4402. DOI: 10.1109/MEI.2018.8246118. URL: https://ieeexplore.ieee.org/document/8246118/?arnumber=8246118 (visited on 08/05/2024).

[42] Zhiwen Huang et al. “The degradation of silicone rubber composites with ZnO microvaristors under impulse voltage”. en. In: *Journal of Physics D: Applied Physics* 55.35 (June 2022). Publisher: IOP Publishing, p. 355501. ISSN: 0022-3727. DOI: 10.1088/1361-6463/ac767d. URL: https://doi.org/10.1088/1361-6463/ac767d (visited on 10/31/2025).

[43] Zichen Zhang et al. “Field-Grading Effect of a Nonlinear Resistive Polymer-Nanoparticle Composite Triple-Point Coating on Direct-Bond Copper Substrates for Packaging Medium-Voltage Power Devices”. In: *2022 IEEE Electrical Insulation Conference (EIC)*. ISSN: 2576-6791. June 2022, pp. 439–442. DOI: 10.1109/EIC51169.2022.9833185. URL: https://ieeexplore.ieee.org/abstract/document/9833185 (visited on 10/20/2023).

[44] Zichen Zhang et al. “Package Design of a Double-Side Cooled 20-kV Gallium Nitride Diode Module With Improved Insulation by Nonlinear Resistive Polymer-Nanoparticle Coating”. In: *2023 IEEE Applied Power Electronics Conference and Exposition (APEC)*. ISSN: 2470-6647. Mar. 2023, pp. 1622–1626. DOI: 10.1109/APEC43580.2023.10131480. URL: https://ieeexplore.ieee.org/abstract/document/10131480 (visited on 10/20/2023).

[45] Zichen Zhang et al. “Packaging of a 15-kV Silicon Carbide MOSFET With Insulation Enhanced by a Nonlinear Resistive Polymer-Nanoparticle Coating”. In: *2022 IEEE Energy Conversion Congress and Exposition (ECCE)*. ISSN: 2329-3748. Oct. 2022,

pp. 1–4. DOI: 10.1109/ECCE50734.2022.9947881. URL: https://ieeexplore.ieee.org/abstract/document/9947881 (visited on 10/20/2023).

[46] Yin Huang et al. "Surface flashover performance of epoxy resin microcomposites improved by electron beam irradiation". In: *Applied Surface Science* 406 (June 2017), pp. 39–45. ISSN: 0169-4332. DOI: 10.1016/j.apsusc.2017.02.093. URL: https://www.sciencedirect.com/science/article/pii/S0169433217304555 (visited on 12/12/2024).

[47] Boxue Du et al. "Carrier mobility and trap distribution dependent flashover characteristics of epoxy resin". en. In: *IET Generation, Transmission & Distribution* 12.2 (2018). _eprint: https://onlinelibrary.wiley.com/doi/pdf/10.1049/iet-gtd.2017.0984, pp. 466–471. ISSN: 1751-8695. DOI: 10.1049/iet-gtd.2017.0984. URL: https://onlinelibrary.wiley.com/doi/abs/10.1049/iet-gtd.2017.0984 (visited on 12/12/2024).

[48] Honglu Guan et al. "Surface potential decay and DC surface flashover characteristics of DBD plasma-treated silicone rubber". en. In: *Nanotechnology* 31.42 (July 2020). Publisher: IOP Publishing, p. 424005. ISSN: 0957-4484. DOI: 10.1088/1361-6528/aba29f. URL: https://dx.doi.org/10.1088/1361-6528/aba29f (visited on 12/12/2024).

[49] Cheng Zhang et al. "Atmospheric pressure plasmas and direct fluorination treatment of Al2O3-filled epoxy resin: A comparison of surface charge dissipation". In: *Surface and Coatings Technology* 362 (Mar. 2019), pp. 1–11. ISSN: 0257-8972. DOI: 10.1016/j.surfcoat.2019.01.081. URL: https://www.sciencedirect.com/science/article/pii/S0257897219300982 (visited on 12/12/2024).

[50] B. X. Du, H. C. Liang, and J. Li. "Interfacial E-field self-regulating insulator considered for DC GIL application". In: *IEEE Transactions on Dielectrics and Electrical Insulation* 26.3 (June 2019). Conference Name: IEEE Transactions on Dielectrics and Electrical

Insulation, pp. 801–809. ISSN: 1558-4135. DOI: 10.1109/TDEI.2018.007761. URL: https://ieeexplore.ieee.org/document/8726027 (visited on 12/11/2024).

[51] B. X. Du et al. "Temperature dependent surface potential decay and flashover characteristics of epoxy/SiC composites". In: *IEEE Transactions on Dielectrics and Electrical Insulation* 25.2 (Apr. 2018). Conference Name: IEEE Transactions on Dielectrics and Electrical Insulation, pp. 631–638. ISSN: 1558-4135. DOI: 10.1109/TDEI.2017.006872. URL: https://ieeexplore.ieee.org/document/8341657 (visited on 12/11/2024).

[52] Hucheng Liang et al. "Effects of non-linear conductivity on charge trapping and detrapping behaviours in epoxy/SiC composites under DC stress". en. In: *IET Science, Measurement & Technology* 12.1 (2018). _eprint: https://onlinelibrary.wiley.com/doi/pdf/10.1049/iet-smt.2016.0528, pp. 83–89. ISSN: 1751-8830. DOI: 10.1049/iet-smt.2016.0528. URL: https://onlinelibrary.wiley.com/doi/abs/10.1049/iet-smt.2016.0528 (visited on 12/11/2024).

[53] Zijun Pan et al. "Contribution of nano-SiC/epoxy coating with nonlinear conduction characteristics to surface charge accumulation under DC voltage". en. In: *Journal of Physics D: Applied Physics* 53.36 (June 2020). Publisher: IOP Publishing, p. 365303. ISSN: 0022-3727. DOI: 10.1088/1361-6463/ab90b1. URL: https://dx.doi.org/10.1088/1361-6463/ab90b1 (visited on 12/11/2024).

[54] Jianyi Xue et al. "Enhancing flashover performance of alumina/epoxy spacers by adaptive surface charge regulation using graded conductivity coating". en. In: *Nanotechnology* 31.36 (June 2020). Publisher: IOP Publishing, p. 364002. ISSN: 0957-4484. DOI: 10.1088/1361-6528/ab938f. URL: https://dx.doi.org/10.1088/1361-6528/ab938f (visited on 12/11/2024).

[55] Jian-Yi Xue et al. "The regulation mechanism of SiC/epoxy coatings on surface charge behavior and flashover performance of epoxy/alumina spacers". en. In: *Journal of*

Physics D: Applied Physics 52.40 (July 2019). Publisher: IOP Publishing, p. 405502. ISSN: 0022-3727. DOI: 10.1088/1361-6463/ab3001. URL: https://dx.doi.org/10.1088/1361-6463/ab3001 (visited on 12/11/2024).

[56] Felix Hoffmann, Stefan Schmitt, and Nando Kaminski. *Reliability of SiC MOSFET power modules under consecutive H3TRB and Power Cycling Stress*. Oct. 2022.

[57] S. Kremp and O. Schilling. "Humidity robustness for high voltage power modules: Limiting mechanisms and improvement of lifetime". In: *Microelectronics Reliability*. 29th European Symposium on Reliability of Electron Devices, Failure Physics and Analysis (ESREF 2018) 88-90 (Sept. 2018), pp. 447–452. ISSN: 0026-2714. DOI: 10.1016/j.microrel.2018.06.043. URL: https://www.sciencedirect.com/science/article/pii/S0026271418304591 (visited on 10/30/2023).

[58] Charalampos Papadopoulos et al. "The influence of humidity on the high voltage blocking reliability of power IGBT modules and means of protection". In: *Microelectronics Reliability*. 29th European Symposium on Reliability of Electron Devices, Failure Physics and Analysis (ESREF 2018) 88-90 (Sept. 2018), pp. 470–475. ISSN: 0026-2714. DOI: 10.1016/j.microrel.2018.07.130. URL: https://www.sciencedirect.com/science/article/pii/S0026271418307108 (visited on 10/30/2023).

[59] Diane-Perle Sadik et al. "Humidity testing of SiC power MOSFETs". In: *2016 IEEE 8th International Power Electronics and Motion Control Conference (IPEMC-ECCE Asia)*. May 2016, pp. 3131–3136. DOI: 10.1109/IPEMC.2016.7512796. URL: https://ieeexplore.ieee.org/document/7512796 (visited on 10/28/2023).

[60] Peng Wang et al. "The Influence of Relative Humidity on Partial Discharge and Endurance Features under Short Repetitive Impulsive Voltages". In: *2018 IEEE Conference on Electrical Insulation and Dielectric Phenomena (CEIDP)*. ISSN: 2576-

2397. Oct. 2018, pp. 506–509. DOI: 10.1109/CEIDP.2018.8544905. URL: https://ieeexplore.ieee.org/document/8544905 (visited on 07/29/2024).

[61] Yanhao Wang et al. "Advanced Power Cycling Test Integrated With Voltage, Current, Temperature, and Humidity Stress". In: *IEEE Transactions on Power Electronics* 38.6 (June 2023). Conference Name: IEEE Transactions on Power Electronics, pp. 7685–7696. ISSN: 1941-0107. DOI: 10.1109/TPEL.2023.3246498. URL: https://ieeexplore.ieee.org/document/10049154 (visited on 10/31/2023).

[62] Zhiliang Xu et al. "Humidity related failure mechanism of IGBTs considering dynamic avalanche". In: *Microelectronics Reliability* 151 (Dec. 2023), p. 115241. ISSN: 0026-2714. DOI: 10.1016/j.microrel.2023.115241. URL: https://www.sciencedirect.com/science/article/pii/S0026271423003414 (visited on 10/31/2023).

[63] Christian Zorn and Nando Kaminski. "Acceleration of temperature humidity bias (THB) testing on IGBT modules by high bias levels". In: vol. 2015. June 2015, pp. 385–388. DOI: 10.1109/ISPSD.2015.7123470.

[64] Brian T. DeBoi et al. "Analysis of Moisture-Induced Void Formations within Silicon Carbide Power Modules". In: *PCIM Europe 2023; International Exhibition and Conference for Power Electronics, Intelligent Motion, Renewable Energy and Energy Management*. May 2023, pp. 1–8. DOI: 10.30420/566091121. URL: https://ieeexplore.ieee.org/document/10173220 (visited on 10/28/2023).

[65] K. Hatori and Keiichi Nakamura. "Humidity Robustness Verification Test for HVIGBT Modules". In: 2020. URL: https://www.semanticscholar.org/paper/Humidity-Robustness-Verification-Test-for-HVIGBT-Hatori-Nakamura/46117b90c949cc9b340265dec4e (visited on 10/30/2023).

[66] Keiichi Nakamura et al. "The test method to confirm robustness against condensation". In: *2019 21st European Conference on Power Electronics and Applications (EPE '19*

ECCE Europe). Sept. 2019, P.1–P.8. DOI: 10.23919/EPE.2019.8915482. URL: https://ieeexplore.ieee.org/document/8915482 (visited on 10/30/2023).

[67] O. Schilling et al. "Generating and characterizing condensation phenomena in power modules". In: *Microelectronics Reliability*. Proceedings of ESREF 2021, 32nd European Symposium on Reliability of Electron Devices, Failure Physics and Analysis 126 (Nov. 2021), p. 114280. ISSN: 0026-2714. DOI: 10.1016/j.microrel.2021.114280. URL: https://www.sciencedirect.com/science/article/pii/S0026271421002468 (visited on 10/30/2023).

[68] Nobuhiko Tanaka et al. "Robust HVIGBT module design against high humidity". In: 2015. URL: https://www.semanticscholar.org/paper/Robust-HVIGBT-module-design-against-high-humidity-Tanaka-Ota/33db4ec2d73f84d941bf540eda9bac7fb1fd16b0 (visited on 10/30/2023).

[69] Christian Zorn, Nando Kaminski, and Michel Piton. "Impact of Humidity on Railway Converters". In: May 2017.

[70] Michiel van Soestbergen and Amar Mavinkurve. "Anomalous water absorption by microelectronic encapsulants due to hygrothermal-induced degradation". en. In: *Journal of Applied Polymer Science* 131.24 (2014). _eprint: https://onlinelibrary.wiley.com/doi/pdf/10.1002/a ISSN: 1097-4628. DOI: 10.1002/app.41192. URL: https://onlinelibrary.wiley.com/doi/abs/10.1002/app.41192 (visited on 10/10/2024).